



Ana Sofia Taborda Martins Pereira

Licenciada em Ciências de Engenharia Biomédica

Development of a Cellulose Acetate Multisensorial Membrane

Dissertação para obtenção do Grau de Mestre em
Engenharia Biomédica

Orientador: Isabel Ferreira, Professora Associada,
DCM-FCT/UNL

Co-orientador: Ana Baptista, Investigadora Pós-Douto-
ramento, DCM-FCT/UNL



FACULDADE DE
CIÊNCIAS E TECNOLOGIA
UNIVERSIDADE NOVA DE LISBOA

Setembro, 2017

Development of a Cellulose Acetate Multisensorial Membrane

Copyright © Ana Sofia Taborda Martins Pereira, Faculdade de Ciências e Tecnologia, Universidade Nova de Lisboa.

A Faculdade de Ciências e Tecnologia e a Universidade Nova de Lisboa têm o direito, perpétuo e sem limites geográficos, de arquivar e publicar esta dissertação através de exemplares impressos reproduzidos em papel ou de forma digital, ou por qualquer outro meio conhecido ou que venha a ser inventado, e de a divulgar através de repositórios científicos e de admitir a sua cópia e distribuição com objectivos educacionais ou de investigação, não comerciais, desde que seja dado crédito ao autor e editor.

Às mulheres da minha vida: Isabel, Elsa e Irene

Aknowledgements

Em primeiro lugar, quero agradecer à minha orientadora, Professora Isabel Ferreira, por me ter dado a oportunidade de concretizar este projecto. Muito obrigada pela motivação, disponibilidade, apoio e conhecimento transmitido.

À minha co-orientadora, Doutora Ana Baptista, agradeço-lhe toda a boa disposição, a disponibilidade demonstrada, toda a paciência e constante preocupação e dedicação. Mesmo quando os resultados não eram os mais promissores, teve sempre uma palavra de incentivo. Obrigada por todo o conhecimento transmitido.

Aos meus colegas, e agora amigos, de laboratório – os meus sinceros agradecimentos. Foi um prazer partilhar com cada um de vocês, de maneiras diferentes, este capítulo que agora me vejo completar. Obrigada pelo companheirismo e ajuda, em especial ao David Sousa, que ganhou um lugar especial no meu coração, agora insubstituível.

À minha mãe, Elsa, e também à minha avó, Isabel, agradeço-vos pela pessoa que sou e o dever a vocês. Pela educação que me deram ao longo da vida, pela alegria que sempre me transmitiram e por todo o amor que me deram. Obrigada por estarem sempre presentes, mesmo não estando junto a mim. São ambas um exemplo para mim, tenho-vos como as pessoas mais carinhosas e bondosas que conheci. Mãe, és a minha razão de viver, amo-te muito!

À minha tia, Irene, obrigada pela oportunidade de realizar esta longa caminhada, pelo apoio incontestável, por toda a força, por me fazer acreditar que

irei muito mais além e pela inquestionável motivação. O mais sincero de todos os obrigados a si, a quem admiro a forte personalidade e a quem estimo toda a amizade.

Ao Miguel Dias, Mimi, que foi o meu pilar durante praticamente dez anos inteiros, um obrigada infinito. Sem ti, a minha sanidade mental não teria sido preservada. Obrigada por todo o amor que me deste, por todo o apoio incondicional. Não tenho palavras que cheguem para ti, contigo cresci e aprendi muito mais do que poderia imaginar.

Um obrigada do fundo do coração à Tia São e ao Tio Zé, os quais considero uns segundos pais, por todo o apoio e carinho com que sempre me trataram.

Não posso deixar de agradecer às amigas FCTenses, Joana Reis e Anayza Soares, bem como aos amigos mais procrastinadores: Nana e Rômulo. O meu percurso académico foi a festa que foi graças a vocês! Levo-vos no coração!

E por fim, mas não menos importante, aos amigos para sempre, às luzes da minha vida, às almas penadas mais divertidas e cúmplices que tive a honra de conhecer: Renata e André, o meu enorme obrigada por serem omnipresentes. Adoro-vos até à Lua!

Abstract

Biological fluids are the most measured media to monitor metabolites like glucose. Glucose measuring is important since it requires routine track for patients undergoing self-testing, like patients diagnosed with pathologies that require daily control of these metabolites or people who have problems with blood collection like haemophiliacs. It can prove to be painful and stressful collecting samples since most methods are invasive.

The well-being and life quality of these patients can be improved by performing non-invasive tests to body fluids at the surface of the skin without ever losing biochemical profiling. Sweat and saliva can be collected more frequently this way, proving less painful and less stressful to the patients.

By combining different biosensing functionalities in a unique membrane, in order to make it multisensorial, and integrate it in a wearable device which can be used on the skin's surface as a band-aid, it's possible to perform auto diagnosis keeping in mind a reduced cost policy, portability and ecology.

In this work, cellulose acetate membranes, produced by electrospinning, were used in the construction of electrochemical devices and these were tested for pH and different concentrations of glucose.

Keywords: biosensor, non-enzymatic, non-invasive, glucose, pH, cellulose acetate, electrospinning, polymer, polyaniline, polypyrrole, PEDOT.

Resumo

Fluidos biológicos são os meios mais medidos quando se trata de monitorizar metabolitos como a glucose. A sua medição é importante para pacientes que necessitem de realizar uma monitorização contínua, como é o caso de pessoas que sofrem de doenças que requerem autoexames ou mesmo pessoas com fobias, como no caso de hemofílicos. Para eles, tais tarefas mostram-se penosas e dolorosas pois a maior parte dos métodos utilizados para recolha de amostras são invasivos.

É possível melhorar o bem-estar e a qualidade de vida desses pacientes através de testes não invasivos a fluidos corporais à superfície da pele sem perder o perfil bioquímico. Amostras de saliva e suor podem ser recolhidas de formas mais frequentes do que o sangue, trazendo menos complicações aos pacientes.

Ao combinar diferentes funcionalidades numa membrana que actua como um biossensor de forma a integrá-la numa plataforma que se possa colocar sobre a pele como um penso, é possível realizar um autodiagnóstico tendo em conta uma política de custos reduzidos, portabilidade e de ecologia.

Neste trabalho foram utilizadas membranas de acetato de celulose, produzidas por *eletrospinning*, na construção de dispositivos eletroquímicos e estes testados na detecção de pH e diferentes concentrações de glucose.

Palavras-chave: biossensor, não-enzimático, não invasivo, glucose, pH, acetato de celulose, electrofiação, polímero, polianilina, polipirrol, PEDOT.

Contents

LIST OF FIGURES	XV
LIST OF TABLES	XIX
ACRONYMS	XXI
INTRODUCTION.....	1
MATERIALS AND METHODS.....	9
RESULTS AND DISCUSSION.....	23
CONCLUSIONS.....	59
BIBLIOGRAPHY.....	63
APPENDICES	69

List of Figures

FIGURE 1.1 - PICTURE OF LEE ET AL.'S WEARABLE SWEAT MONITORING PATCH	7
FIGURE 1.2 - CELLULOSE ACETATE STRUCTURE	8
FIGURE 2.1 - SCHEMATIC DIAGRAM OF A CONVENTIONAL ELECTROSPINNING SETUP	10
FIGURE 2.2 – SCHEMATIC OF THE PREPARATION PROCEDURE OF PANI FUNCTIONALIZED CELLULOSE NANOFIBERS	11
FIGURE 2.3 – OPTICAL CAMERA IMAGE OF AN EXAMPLE PREPARATION WITH DIFFERENT FUNCTIONALIZED CA MEMBRANES.	15
FIGURE 2.4 - EXAMPLE OF A MICROSCOPE SLIDE CONTAINING SMALL SAMPLES OF FUNCTIONALIZED CA MEMBRANES MEASURE POTENTIOSTATIC EIS	17
FIGURE 2.5 - SCHEMATIZATION OF THE CHOSEN ELECTRODE CONFIGURATION USED IN THE ELECTRO-CHEMICAL MEASUREMENTS.....	19
FIGURE 2.6 - PICTURE OF THE ELECTROCHEMICAL TEFLON-MADE CELL USED ON THE CYCLIC VOLTAMMETRY STUDIES	20
FIGURE 3.1 – SEM IMAGES OF CA ELECTROSPUN MEMBRANE (I) BEFORE AND (II) AFTER IMMERSION ON A 0.1M NAOH (PH 13) ELECTROLYTE SOLUTION.....	31
FIGURE 3.2 – SEM IMAGES OF CA ELECTROSPUN MEMBRANE FUNCTIONALIZED WITH PANI (I) BEFORE AND (II) AFTER IMMERSION ON A 0.1M NAOH (PH 13) ELECTROLYTE SOLUTION.....	31
FIGURE 3.3 – SEM IMAGES OF CA ELECTROSPUN MEMBRANE FUNCTIONALIZED WITH PPY (I) BEFORE AND (II) AFTER IMMERSION ON A 0.1 M NAOH (PH 13) ELECTROLYTE SOLUTION.....	31
FIGURE 3.4 – SEM IMAGES OF CA ELECTROSPUN MEMBRANE FUNCTIONALIZED WITH PEDOT (I) BEFORE AND (II) AFTER IMMERSSED ON A 0.1M NAOH (PH 13) ELECTROLYTE SOLUTION	28
FIGURE 3.5 – ATR-FTIR SPECTRA OF CA, PANI FUNCTIONALIZED CA, PPY FUNCTIONALIZED CA AND PEDOT FUNCTIONALIZED CA MEMBRANES.....	30
FIGURE 3.6 - REPRESENTATIVE I-V CURVE OBTAINED FOR PEDOT/CA MEMBRANE....	32
FIGURE 3.7 – SEM IMAGES OF CA ELECTROSPUN MEMBRANE FUNCTIONALIZED WITH PPY (I) BEFORE AND (II) AFTER IMMERSION ON A 0.1 M NAOH (PH 13) ELECTROLYTE SOLUTION.....	34
FIGURE 3.8 – SEM IMAGES OF CA ELECTROSPUN MEMBRANE FUNCTIONALIZED WITH PPY (I) BEFORE AND (II) AFTER IMMERSION ON A 0.1 M NAOH (PH 13) ELECTROLYTE SOLUTION.....	34

FIGURE 3.9 - EIS FITTING CURVE OF A PPy/CA MEMBRANE (RED DOTS) AND ITS EIS EXPERIMENTAL CURVE (BLUE).....	35
FIGURE 3.10 - CIRCUIT MODEL OF A PPy/CA MEMBRANE AT HIGH FREQUENCY CAPACITANCE.....	35
FIGURE 3.11 - EIS FITTING OF A PEDOT/CA MEMBRANE (RED DOTS) AND ITS EIS EXPERIMENTAL CURVE (BLUE).....	36
FIGURE 3.12 - CIRCUIT MODEL OF A PEDOT/CA MEMBRANE AT HIGHLY CONDUCTIVE DC.	36
FIGURE 3.13 - EIS FITTING OF A LESS CONDUCTIVE AT DC PEDOT/CA MEMBRANE (RED DOTS) AND ITS EXPERIMENTAL CURVE (BLUE).....	37
FIGURE 3.14 - CIRCUIT MODEL OF A PEDOT/CA MEMBRANE AT HIGH FREQUENCY CAPACITANCE SHOWING THE NON-COVERED INSULATING BULK OF THE CA FIBERS WITH PEDOT.....	37
FIGURE 3.15 - PANI/CA (I), PPy/CA (II) AND PEDOT/CA (III) VOLTAMMOGRAMS AT 20, 40, 80 AND 100 MV/S AND (IV) SHOWS THE DEPENDENCE OF THE SCAN RATE TO PANI/CA, PPy/CA AND PEDOT/CA'S PEAK CURRENTS.....	40
FIGURE 3.16 - PANI/CA (I), PPy/CA (II) AND PEDOT/CA (III) VOLTAMMOGRAMS AT 80 mV/S USING DIFFERENT CONCENTRATIONS OF GLUCOSE 0.1 M NaOH SOLUTION AS ELECTROLYTE.....	43
FIGURE 3.17 - PLOTS OF GLUCOSE CONCENTRATION VERSUS ANODIC PEAK CURRENT (I), ANODIC PEAK POTENTIAL (II), CATHODIC PEAK CURRENT (III), CATHODIC PEAK POTENTIAL (IV), OF THE PANI/CA MEMBRANES	45
FIGURE 3.18 - PLOTS OF GLUCOSE CONCENTRATION VERSUS ANODIC PEAK CURRENT (I), ANODIC PEAK POTENTIAL (II), CATHODIC PEAK CURRENT (III), CATHODIC PEAK POTENTIAL (IV), OF THE PPy/CA MEMBRANES	46
FIGURE 3.19 - PLOTS OF GLUCOSE CONCENTRATION VERSUS ANODIC PEAK CURRENT WITH A FITTING DONE EXCLUDING DATA CIRCLED IN RED (I), ANODIC PEAK POTENTIAL (II), CATHODIC PEAK CURRENT (III), CATHODIC PEAK POTENTIAL (IV), OF THE PEDOT/CA MEMBRANES.....	47
FIGURE 3.20 - CYCLIC VOLTAMMOGRAMS FOR PANI/CA (I), PPy/CA (II) AND PEDOT/CA (III), ALL RAN AT 80 mV/S WITH THREE DIFFERENT ARTIFICIAL SWEAT SIMULATING ELECTROLYTES WITH PH 4 (AATCC), PH 6 (ISO) AND PH 8 (ISO).....	51
FIGURE 3.21 - EQUATION EXPLAINING PANI'S ELECTROCHEMICAL BEHAVIOUR.....	52
FIGURE 3.22 - SCHEME REPRESENTING THE OXIDATION OF PYRROLE RINGS AND THEIR LOSS OF CONJUGATION WHEN THE FORMING OF CARBONYL GROUPS OCCUR [48].....	52
FIGURE 3.23 - CHRONOAMPEROGRAMS OF PANI/CA (I), PPy/CA (II) AND PEDOT/CA (III) FOR DIFFERENT GLUCOSE CONCENTRATIONS.....	54
FIGURE 3.24 - CHRONOAMPEROGRAMS OF PANI/CA (I), PPy/CA (II) AND PEDOT/CA (III) FOR DIFFERENT ARTIFICIAL SWEAT SOLUTIONS.....	55
A.1 - CYCLIC VOLTAMMETRY EXPERIMENTAL SETUP RESULTS WITHOUT A CARBON STRIP INSIDE THE TEFLON-MADE CELL, WITH A CARBON STRIP ON TOP OF THE MEMBRANE AND BENEATH IT.....	69
A.2 - CYCLIC VOLTAMMOGRAMS FOR PANI/CA, PPy/CA AND PEDOT/CA USING DIFFERENTLY CONCENTRATED SOLUTIONS OF GLUCOSE ELECTROLYTE.....	70
A.3 - ARTIFICIAL SWEAT CYCLIC VOLTAMMETRY OF PANI/CA, PPy/CA AND PEDOT/CA WITH DIFFERENT RANGES OF APPLIED POTENTIAL	71
A.4 - CHRONOAMPEROMETRY FOR PANI/CA WITH ARTIFICIAL SWEAT SOLUTIONS TESTING DIFFERENT METHODOLOGIES.....	72

List of Tables

TABLE 1.1 – TABLE SUMMARIZING DIFFERENT TYPES OF BIOSENSORS.....	3
TABLE 2.1 - ELECTROSPINNING PARAMETERS USED TO PRODUCE CA ELECTROSPUN MEMBRANES.....	10
TABLE 2.2 – CHEMICAL COMPOSITION OF THE THREE TYPES OF ARTIFICIAL SWEAT SOLUTIONS USED FOR THE DEVICE’S ELECTROCHEMICAL MEASUREMENTS	18
TABLE 2.3 - AVERAGE SAMPLE THICKNESS OF THE ELECTRODES USED IN CYCLIC VOLTAMMETRY	20
TABLE 3.1 - AVERAGE CA FIBER DIAMETERS WHEN FUNCTIONALIZED WITH PANI, PPy AND PEDOT BEFORE AND AFTER IMMERSION IN 0.1 M NaOH (pH 13)	34
TABLE 3.2 – CONDUCTIVITY OF PANI/CA, PPy/CA AND PEDOT/CA MEMBRANES, BEFORE AND AFTER BEING DIPPED IN 0.1 M NaOH SOLUTION, RELATED TO THE CORRESPONDING MEMBRANE AVERAGE THICKNESS (TAV)	44
TABLE 3.3 – DIFFERENT CONCENTRATIONS OF GLUCOSE 0.1 M NaOH SOLUTION AND ITS CORRESPONDING FUNCTIONALIZED MEMBRANE PEAK POTENTIALS	43
TABLE 3.4 – TABLE SUMMARIZING PANI/CA, PPy/CA, PEDOT/CA FUNCTIONAL GROUPS, FITTING EQUATIONS, COEFFICIENTS OF DETERMINATION AND PEAK TYPE.....	48
TABLE 3.5 – TABLE COMPRISING THE STABILIZATION CURRENT IN μA TAKEN FROM THE CHRONOAMPEROGRAMS FOR PANI/CA, PPy/CA AND PEDOT/CA, AS FUNCTION OF DIFFERENT ARTIFICIAL SWEAT SOLUTION pH	55

Acronyms

WHO	World Health Organization
CA	Cellulose Acetate
PPy	Polypyrrole
PEDOT	Poly(3,4-ethylenedioxythiophene)
PANI	Polyaniline
PANI/CA	Polyaniline functionalized cellulose acetate membrane
PPy/CA	Polypyrrole functionalized cellulose acetate membrane
PEDOT/CA	Poly(3,4-ethylenedioxythiophene) functionalized cellulose acetate membrane
DMAc	Dimethylacetamide
GOx	Glucose Oxidase
ISO	International Organization for Standardization
AATCC	American Association of Textile Chemists and Colorists
SEM	Scanning Electron Microscopy
ATR	Attenuated Total Reflectance
FTIR	Fourier Transform Infrared

IR	Infrared Radiation
<i>I-V</i>	Curves Current-Voltage Characteristic Curves
EIS	Electrochemical Impedance Spectroscopy
AC	Alternating Current
WS	Working Sense
WE	Working Electrode
CE	Counter Electrode
RE	Reference Electrode
CV	Cyclic Voltammetry
D_{av}	Average Diameter
Mw	Molecular weight
T_{Av}	Average Thickness
Z	Complex Impedance
Y	Complex Admittance
X	Total Imaginary Reactance
XC	Capacitive component in the complex plane of the total imaginary reactance
XL	Inductive component in the complex plane of the total im- aginary reactance
ω	Angular Frequency
φ_Z	Phase Angle of the Impedance Magnitude
φ_Y	Phase Angle of the Admittance Magnitude
σ	Conductivity, σ in Siemens per centimeter (S/cm)



Introduction

1.1 - Motivation

Present day effective healthcare demands require medical diagnostics laboratories to use accurate, fast and inexpensive devices in a routinely way.

Biological sensing devices are widely used in clinical diagnosis as integrated biomedical systems mainly due to their fast response and reduced size. This makes them highly distinguishable in immediate testing through their sensitivity and specificity, thus providing viable solutions to contemporary healthcare industry needs.

The need to expand and spread clinical analysis in an independent way to doctor's clinics and patients self-testing at home has been increasing, thus, continuous efforts to provide ready-to-go care and new concepts of portable analysis are coming up. Biosensors were made available in the market as a small sized method of rapid detection for that purpose.

Biological fluids as blood, serum and urine are between the most measured media to monitor metabolites such as glucose, urea and lactate. These measurements are important since they require routine track for patients undergoing self-testing. They are also relevant for patients diagnosed with pathologies that require daily control of these metabolites or people who have problems with blood collecting like haemophiliacs. It can prove to be painful and stressful collecting samples since most methods are invasive. There has been an increase in trying to

measure metabolites in body fluids others than blood by non-invasive means in developing biosensors in clinical analysis.

Improving the well-being and life quality of these patients is an attainable possibility - by performing non-invasive tests to body fluids at the surface of the skin without ever losing biochemical profiling. Sweat and saliva can be collected more frequently this way, proving less painful and less stressful to the patients.

By combining different biosensing functionalities in a unique membrane, in order to make it multisensorial, and integrate it in a wearable device which can be used on the skin's surface as a band-aid, a sticker or a temporary tattoo, it's possible to perform auto diagnosis keeping in mind a reduced cost policy, portability and ecology without the physical presence in a clinical analysis laboratory, be it in critical moments or in a daily routine short term monitoring.

In this context, the present work aims the development of a multisensorial membrane that can monitor glucose and pH levels, envisaging patients with pathologies such as diabetes mellitus, which require real time and continuous control of those levels in a fast, painless, safe and simple way.

1.2 - State of the Art

The first concept of biosensor ever was defined by Clark Jr, by publishing his work on oxygen electrodes in the year of 1956. Later, in 1962, he described his first glucose oxidase (GOx) immobilization experience on electrodes, via a dialysis membrane. With that, it was verified that glucose and oxygen concentration are proportional since decreasing of one of them, lessens the other [1].

Clark's original patent states that a number of enzymes can be used to convert electroinactive substrates into electroactive products. The use of two electrodes, having one of them covered with GOx, and differential current measurements helped correct the effect of interference. [1]

Only in 1967, Updike and Hicks made a detailed description of a functional enzymatic electrode, using glucose oxidase in an oxygen sensor. Interest began rising in trying to use it in biotechnological applications of enzyme based sensors, devised on immobilization methods and using oxireductases, polyphenol oxidases, peroxidases and aminooxidases. It was the first generation of biosensors

[2]. Since then, various types of sensors were developed - Table 1.1 summarizes them.

Table 1.1 -Table summarizing different types of biosensors (adapted from [1], [3])

Type of Sensors	Short Description
Tissue-based Sensors	Developed by Diviès and further perfected by Rechnitz. Tissues are from plant and animal sources, with an inhibitor or a substrate as the analyte of interest.
Organelle-based Sensors	Made using membranes, chloroplasts, mitochondria and microsomes. High stability despite longer detection times and reduced specificity.
Immunosensors	Based on the high affinity of antibodies towards antigens for them to interact with the host's immune system.
DNA Biosensors	Diagnose hereditary disease and pathogenic infections, by sequencing and hybridizing DNA. Lund et al. connected DNA to microsphere surfaces and Gambhir et al. first immobilized DNA in polypyrrole films.
Magnetic Biosensors	Miniaturized in size, they detect magnetic nanoparticles in microfluidic channels because of the magnetoresistance effect.
Thermal or Calorimetric Biosensors	Developed by assimilating biosensor materials into physical transducers.
Piezoelectric Biosensors	Two different types: quartz crystal microbalance and surface acoustic wave device.

	Both measure changes in resonance frequency of a piezoelectric crystal due to its structure's mass changes
Optical Biosensors	With a light source, a light beam is generated with defined characteristics to be modulated as it goes through a photodetector.
Genetically-Encoded Biosensors	Using genetic fusion reporters, they are user-friendly, easy to engineer, to manipulate and transfer into cells.
Peptide and Protein Sensors	Manufactured through synthetic chemistry followed by enzymatic labelling with synthetic fluorophores. Utilized to control target activity enhancing signal-to-noise ratio and sensitivity of response through introduction of chemical quenchers and photoactivatable groups.

Biosensors used to be described as compact units of analysis with a biological/biologically-derived sensitive recognition element or associated with a physicochemical transducer. They combined the specificity of the biological molecule along the transducer so that a biological sign could be converted into an optical or electrochemical sign [2], [3]. Whilst a chemical sensor was said to be a miniaturized analytical device than could deliver real time and online information on the presence of specific compounds or ions in complex samples [4].

Nowadays, biosensors have acquired a much wider meaning, with no distinction being made between bio and chemical sensors. A biosensor is any sensor that measures a chemical concentration in a biological system, capable of continuous monitoring, fast and precise analysis, all in a simple and ready-to-use device for non-medical personnel [4].

Metabolite-based biosensors are used to clinically monitor analytes such as blood glucose, urea, lactate, cholesterol or uric acid, which offers advantages in

clinical analysis due to their better sensitivity, reproducibility, easy maintenance and low cost. Different detection methods combined with different sensing strategies make good multiparameter sensors. For example, using electrochemical and fibre-optic technology, one can continuously measure in vivo pH, carbon dioxide partial pressure, oxygen partial pressure and oxygen saturation in human pregnancy [2], [3], [5], [6].

Glucose sensors have long been in development mainly due to *diabetes mellitus*. Despite the challenges yet to overcome regarding accuracy and reliability, glucose biosensor technology has been improved with point-of-care devices, continuous glucose monitoring systems and non-invasive glucose monitoring systems with a wide range of applications that go from fermentation to food quality control [3], [7].

Nowadays, one of world wide's most common endocrine disorders of carbohydrate metabolism is *diabetes mellitus*. Being a major health problem, it has become one of the leading causes of morbidity and mortality with increased prevalence. According to the World Health Organization (WHO), in 2000 there were approximately 171 million people suffering from diabetes, a number that is expected to increase to 366 million by 2030 [3].

Blood glucose concentration needs to be monitored in order to prevent further aggravations of diabetes and achieve glycaemic goals, as it provides information for optimizing patient treatment strategies. Since it is a major diagnosis tool, it has gathered particular interest, hence a series of glucose sensors has been developed and dominates the biosensor market [1], [3], [8].

Despite most of the commercially-used glucose sensors being electrochemical enzymatic style - mainly due to their highly sensitive performance, developing an electrochemical enzyme-free glucose sensor has attracted tremendous research interest as long as non-invasive glucose analysis because of the drawbacks enzymatic style glucose sensors have. Drawbacks such as: complications with the immobilization and stabilization protocol of the enzyme, low stability and reproducibility derived from temperature, pH and humidity and the fact that most enzymes are expensive, leading to high fabrication process costs [6], [9], [10].

Even though portable transdermal glucose sensors manufactured in watch-like devices or in screen-printed enzyme electrode test strips have already been developed, a reliable non-invasive glucose measuring method doesn't exist yet [3].

Most sensors hardly reach the market due to issues regarding accuracy of the electrical contacts on the skin, miniaturization and lack of full portability. Stretchable membranes have been the focus of more recent studies since they can feature small size, lightweight and biocompatibility, which are very hard to achieve in a single device [11]-[13].

Sweat is a much more accessible biological fluid than blood – sweat excreting eccrine glands are all over the human body, which makes it qualifiable for diagnosis of many disease markers such as glucose [8], [14].

Recently, there has been an improvement in glucose-sweat sensing devices. Focusing on the non-invasive characteristic, Russell et al. [8] found a new and innovative approach: tattoo sensing technology using glucose-sensing hydrogel microspheres. This concept was further developed by Zhi et al. [8] with envelopment of the sensors in thin film, fastening the analyte transport through the device.

Diamond et al. [8] assembled a sweat sensing device called SwEatch for sodium analysis with 3D-printed sensor cases and connections, a lithium battery that provided a continuous run for 3 hours.

Sweat-sensing patches first came in 2010, by Heikenfeld et al. [8]. They stimulated sweat production and measured analyte concentrations wirelessly. This information could be transmitted to a smartphone.

A non-invasive sensing device for detecting analytes in sweat via electrochemical sensing was tried out by Wang et al. Later, Gao et al. [8] integrated this idea in a Bluetooth-enabled wristband that detected skin temperature, sodium, potassium, lactate and glucose, using multiple sensors.

More recently, Lee et al. [14] assembled a wearable and disposable sweat monitoring device with a microneedle-based transdermal drug delivery module which could perform, as a whole, by doing an electrochemical analysis of sweat

using soft bioelectronics on human skin. A picture of the device is shown in Figure 1.1.

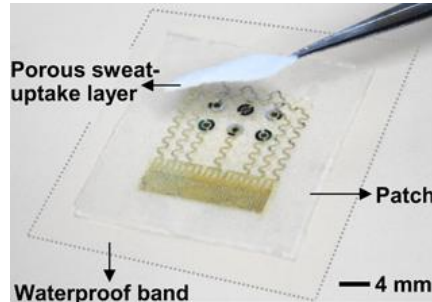


Figure 1.1 - Picture of Lee et al.'s wearable sweat monitoring patch (adapted from [14])

For this project, the relevance of developing an electrochemical sensing platform that uses non-invasive sweat analysis to monitor glucose and pH, so that it can be further developed to possibly integrate a patch-like device in future studies was mainly to miniaturize diagnostic tools and make them easy and ready to use by people in need of such care, like *diabetes mellitus* patients. The innovation comes with the choice of materials to be used. Organic and biocompatible polymers were selected to integrate the platform sensing bulk. This way, not only a sustainable policy was carried out but also a reduced economic investment was made.

Nowadays, sustainable and renewable source derived products have gathered attention since they are less harmful to the planet's ecosystems.

Cellulose is an abundant biopolymeric composite that occurs naturally and, despite its toxic extracting procedures, it's biodegradable and recyclable as it comes mostly from wood, cotton and algae. Its fabrication process has been wide studied and established with a long-time basis of procedure. Cellulose is made of repeating glucopyranosyl rings and can be chemically modified. These are some of the attributes that turn this polymer into one of the core elements of low cost disposable devices [15]-[17].

Cellulose esters come from chemically modified cellulose. When they biodegrade, depending on their degree of esterification, a number of glucopyra-

nosyl's rings hydroxyl groups are replaced by ester groups. They have high water permeability [17], [18]. One of them is cellulose acetate (CA) and was the chosen polymer to use as the biocompatible organic matrix to be functionalized by three different conductive polymers. CA structure is represented in Figure 1.2. Conducting polymers ensure electron conductivity when doped. Doping is performed by means of chemical or electrochemical oxidation or reduction, resulting in the acquisition of positive and negative charges by the polymeric chains. Due to their easier synthesis pathway, biocompatibility and good conductivity, polymers such as Polyaniline (PANI), Polypyrrole (PPy) and Poly(3,4-ethylenedioxythiophene) (PEDOT) have been extensively studied for medical applications [19]-[24].

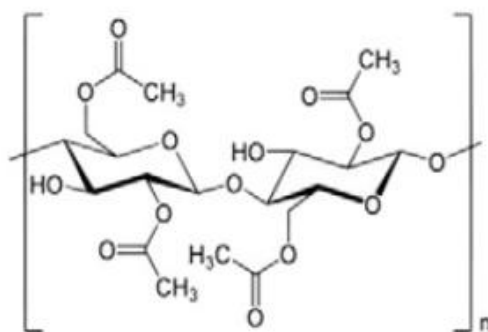


Figure 1.2 - Cellulose acetate structure (adapted from [25])

Electrospinning is a technology that uses electrostatic forces to produce different polymer fibers ranging from nanometers to micrometers via polymer solutions otherwise not attainable through standard mechanical fiber-spinning techniques, which rely on the mechanical effects such as thermal and structural ones to determine fiber properties. It is an adequate technique to employ on cellulose acetate and turn it into a viable matrix for *in situ* polymerizations with conductive polymers [26].

Materials and Methods

This chapter describes, in detail, the preparation of the multisensorial membrane. First, cellulose acetate membranes were electrospun, then functionalized with conductive polymers and finally, tested to electrolytes using different solutions.

2.1 Preparation of Cellulose Acetate electrospun membranes

Cellulose acetate (CA) membranes were produced via electrospinning technique based on parameters optimized in previous studies. A CA solution [12% (w/w) - Mn ~ 50000, 20 - 40% acetyl groups, Sigma-Aldrich] in 2:1 acetone:DMAc solvent mixture was prepared and loaded into a 1ml syringe (B. Braun).

A syringe pump (KDS100) was used to control the flow of the polymer solution through a needle (ITEC, Iberiana Technical, Lda., 21G) at a constant rate of 0.2 ml/h. The tip of the needle was connected to the positive pole of a high voltage source (Glassman High Voltage, Inc.) and the grounded collector is a static aluminium foil placed at a distance of 15 cm from the needle's tip - as illustrated in Figure 2.1. In Table 2.1, the electrospinning parameters used to produce the CA electrospun membranes are listed.

When a high voltage is applied, the molecules within the solution are charged creating a repulsive force. The resulting electrostatic repulsive force on

the newly formed Taylor cone, which is higher than the solution's superficial tension, leads to the formation of an electrically charged jet. Since the surface of least potential is the collector, the jet is accelerated in its way. The solvent evaporates along the path and a polymeric nanofiber matrix is randomly deposited on the collector's surface with a thickness that varies according to the deposition time. The resulting membranes had an average thickness of 361.1 ± 64.1 nm since they were deposited for 5 hours straight.

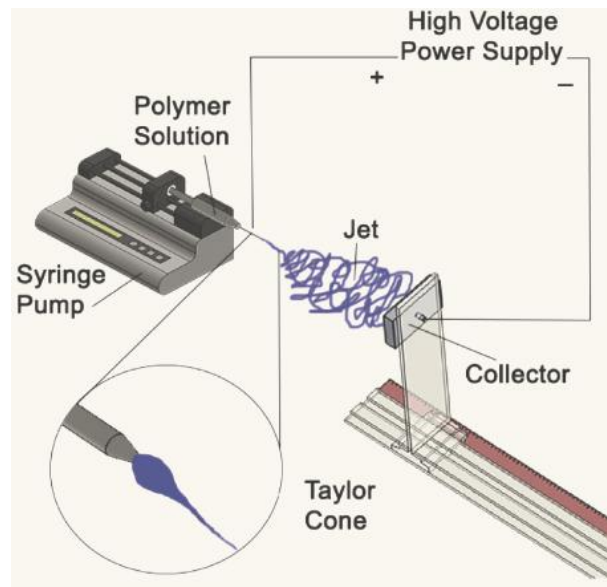


Figure 2.1 - Schematic diagram of a conventional electrospinning setup (adapted from [27])

Table 2.1 - Electrospinning parameters used to produce CA electrospun membranes

Needle Gauge	21
Grounded Collector Distance [cm]	15
Applied voltage [kV]	20
Deposition Time [hours]	5
Relative Humidity [%]	40-60
Temperature [°C]	25

2.2 Functionalization of CA electrospun membranes

The produced CA electrospun membranes were functionalized with polyaniline, polypyrrole or PEDOT all obtained by the polymerization of the monomer (aniline, pyrrole or edot, respectively) using two different approaches: in situ-oxidation in aqueous solution or vapour phase.

2.2.1 In situ oxidation of Aniline in aqueous solution

In order to functionalize the CA electrospun fibers with polyaniline, both aniline (monomer) and ammonium persulfate (oxidizing agent) solutions were prepared according to literature procedure [28], as is schematized in Figure 2.2. A 365 μL of aniline ($\text{C}_6\text{H}_5\text{NH}_2$, Sigma Aldrich, $M_w = 93.13$, 99,50% assay) was dissolved in 10 mL of hydrochloric acid (HCl, 1 M) in an ice bath during 10 minutes. Afterwards, a CA membrane with dimensions of 3 cm \times 2 cm was completely submerged in the previously prepared solution for 10 minutes. A 0.456 g of ammonium persulfate ($(\text{NH}_4)_2\text{S}_2\text{O}_8$, Sigma Aldrich, $M_w = 228.20$, 98% assay) was dissolved in 10 mL of HCl and added dropwise to the monomer solution and left to react for 45 minutes. After polymerization, the CA membrane functionalized with PANI was carefully washed with ultrapure water (Milipore®) and ethanol to stop the reaction and to extract the by-products and residues of the reaction. Later, the membranes were dried at room temperature.

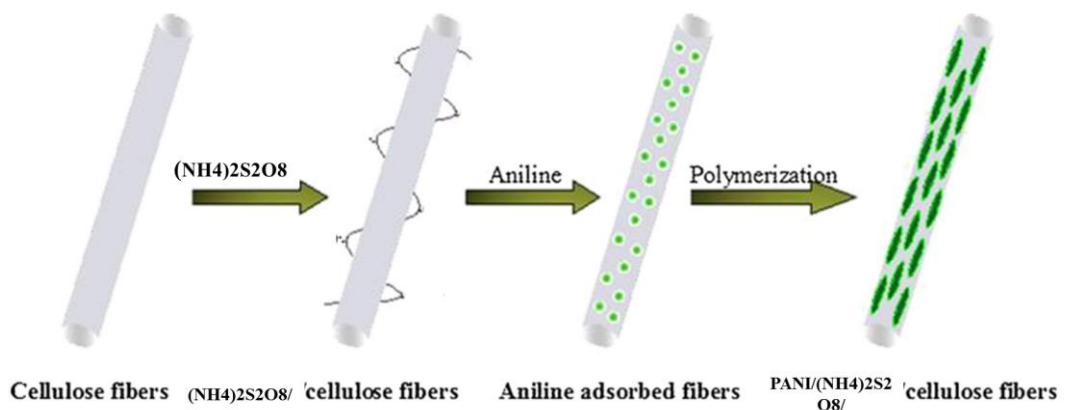


Figure 2.2 - Schematic of the preparation procedure of PANI functionalized cellulose nanofibers (adapted from [19])

2.2.2 *In situ* oxidation of Pyrrole in aqueous solution

To perform this functionalization, pyrrole is used as the monomer and Iron (III) chloride hexahydrate ($\text{FeCl}_3 \cdot 6\text{H}_2\text{O}$, Sigma-Aldrich, $M_w = 270.30$, 98% assay) as an oxidizing agent, in a 1:2 ratio [28].

After preparing a 20 mL aqueous solution of 0.05 M of pyrrole ($\text{C}_4\text{H}_5\text{N}$, Sigma-Aldrich, $M_w = 67.09$ g/mol, 98% assay), a CA membrane with dimensions of 3 cm x 2 cm was added and stirred for 10 minutes to soak the membrane with the monomer.

To initiate the polymerization, 0.134 g of the oxidizing agent were added to the solution and left stirring for 30 minutes. The CA membranes were washed thoroughly with ultrapure water (Milipore®) and ethanol, until no more PPy aggregates were unleashed, and were left to dry at room temperature.

2.2.3 *Vapor-Phase Polymerization of EDOT*

The functionalization of CA electrospun fibers with PEDOT considers two steps: (1) impregnation of the CA membranes with an oxidizing agent and (2) the polymerization of EDOT by evaporating the monomer onto their surface using a sealed chamber.

The solution of oxidizing agent, Iron (III) Chloride Hexahydrate, was prepared by dissolving 0.2 g in 5 mL of water and left stirring for 45 minutes. A 2.5 cm by 1.5 cm CA membrane was submerged in the solution for 15 minutes. After being removed from the solution, it was stretched inside a petri plate, where it was left drying for 24 hours.

Once the CA membranes were dried out, they were hung on the chamber's lid, and sealed inside with 0.5 mL of EDOT ($\text{C}_6\text{H}_6\text{O}_2\text{S}$, Sigma-Aldrich, $M_w = 142.18$ g/mol, 97% assay) on the bottom. The chambers were introduced in an oven (Memmert) at 50°C for 120 minutes. The membranes were taken out, washed with ultrapure water (Milipore®) and ethanol and left to dry at room temperature.

2.3 Characterization of functionalized CA membranes

2.3.1 Scanning Electron Microscopy (SEM)

A high-resolution image of the CA electrospun membranes is possible by SEM. An electron beam is focused to the sample's surface in order to interact with its atoms, ejecting secondary electrons which are detected, translating the signal into an image. Metallic sample coating was required to improve the signal and reduce sample charging.

Sample preparation procedure consisted in cutting small pieces of each membrane, functionalized with each different conductive polymer and without functionalization, placing them on carbon strips on a metallic sample support. The samples were sputtered with carbon thin layer to avoid electrons charging. The surface morphology of CA electrospun membranes was evaluated by SEM, model JEOL 7001.

Fiber diameters were measured from the SEM images using the ImageJ® image processing software. The average diameter of the fibers was estimated from several existing fibers that could be observed on the same level. 10 measurements were made on each fiber per image.

2.3.2 Fourier transform infrared (FTIR) spectroscopy: Attenuated Total Reflectance (ATR)

FTIR provides the membrane's chemical information by generating a spectrum from a sample irradiated by infrared radiation (IR). The absorbed IR radiation excites molecules into a higher vibrational state, by means of a modulated wavelength. The energy difference between that vibrational state and the previous at-rest state is measured as a function of that same wavelength which is characteristic of each molecular structure. The infrared absorption bands identify molecular components and structures, as the FTIR produces interferograms that, once processed with Fourier transforms, result in a single-beam infrared spectrum of intensity *versus* wavenumber.

ATR-FTIR examines chemical bonds at a solid or liquid interface. The probing is done to *in situ* single or multiple layers of absorbed or deposited species. A wavelength dependent infrared radiation interacts with said species, passing

through the ATR crystal, reflecting and then collected by a detector when exiting it. Penetration depth is wavelength of light, angle of incidence and refraction indices dependent.

The spectra were obtained on a Thermo Nicolet 6700 spectrophotometer.

2.3.3 Electrical conductivity

Current-Voltage Characteristic Curves (*I-V* Curves) show the relationship between the current flowing through an electronic device and the applied voltage across its terminals. By applying any voltage value to a resistive element, the resulting current is directly obtained from the *I-V* curve. and so is the power that is dissipated or generated by that same element.

By Ohm's Law,

$$V = RI \quad (2.1)$$

the current through the resistor is a function of the applied voltage, since *I* is proportional to the potential difference, *V*, times the constant of proportionality, $1/R$. So, in an ideal resistance, their relationship is linear, constant and ohmic, making $1/R$ the slope of the straight line that represents the current against the potential difference.

The functionalized membranes' electrical conductivity was measured by obtaining their *I-V* curves and sorting their resistance, hence their conductivity, σ in Siemens per centimeter (S/cm), using the following equation:

$$\sigma = \frac{l}{AR} \quad (2.2)$$

where *l* represents the length of the piece of material, *A* represents the cross-sectional area where the current has passed-through and *R* represents the resistance.

Preparation included taking various samples with all three different functionalized CA membranes, (PANI/CA, PPy/CA and PEDOT/CA), which were cut and immobilized on microscope slides with silver conductive glue, as shown in an example in Figure 2.3. A computerized microprobe (Alessi REL-450) with two micro positioners was used. Five *I-V* curves were obtained for each sample. Conductivity was obtained by calculating their average.



Figure 2.3 - Optical camera image of an example preparation with different functionalized CA membranes, (PANI/CA, PPy/CA and PEDOT/CA), which were cut and immobilized on microscope slides with silver conductive glue to measure electrical conductivity

2.3.4 Electrochemical Impedance Spectroscopy

Electrochemical Impedance Spectroscopy (EIS) helps determining the non-linear behaviour of an electrochemical process as a perturbative characterization of its dynamics. It measures the current that goes through the electrochemical cell after the application of an alternating current (AC) potential as a small excitation signal. This signal can then be analyzed as a Fourier series.

In the present work, however, EIS was used as a counterpart of the electrical conductivity analysis along with the SEM evaluation of the functionalized CA membranes, for modeling the electrochemical systems. Theoretical modelling can explain and predict their behavior and can help designing systems with desired features. Equivalent circuit models were tried out for each functionalized membrane by designing hypothetical electrical circuits that describe the frequency response to the excitation signal [29], [30].

Complex impedance and admittance are defined by

$$Z = R + jX = |Z|e^{j\varphi_Z} \quad (2.3)$$

and

$$Y = |Y|e^{j\varphi_Y} \quad (2.4)$$

where total imaginary reactance X is a sum of the capacitive and inductive components in the complex plane:

$$X = X_L + X_C \quad (2.5)$$

with

$$X_C = -\frac{1}{\omega C} \quad (2.6)$$

and

$$X_L = \omega L \quad (2.7)$$

where ω is the angular frequency.

The potentiostat equipment measures directly either impedance magnitude (absolute value of complex Z) or admittance magnitude (absolute value of complex Y) and phase angle of the impedance (φZ) or admittance (φY) magnitude, respectively, where $Y = 1/Z$ and $\varphi Y = -\varphi Z$.

It is appropriate to consider basic system response at the impedance level. Taking that the overall impedance of the system, Z_z , approaches R_0 at sufficiently low frequencies and R_∞ at sufficiently high ones, one can form the normalized dimensionless quantity

$$I_z = \frac{Z_z - R_\infty}{R_0 - R_\infty} \quad (2.8)$$

If an ideal resistor has zero reactance, whereas ideal inductors and capacitors have zero resistance, then it responds to current only by reactance, which can be both from capacitor or inductor. For this model, it is assumed that there is a reactance of inductor (X_L) and capacitor (X_C) in the circuit. [30]

For the experimental setup, parts of each membrane were cut and glued to microscope slides, using silver glue in a first instance and then carbon paste, since the results were inconclusive for the first one, to go through the potentiostat, as shown in Figure 2.4. Experimental conditions were 1 V DC voltage, 100 mV rms AC voltage, 10^6 Hz of initial frequency and 0.1 Hz of final frequency.

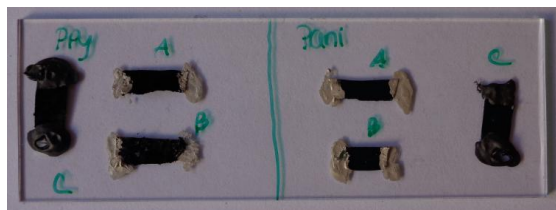


Figure 2.4 - Example of a microscope slide containing small samples of functionalized CA membranes glued either with silver glue (A and B samples) and or with carbon paste (C samples) to measure potentiostatic EIS

2.5 Electrolyte Preparation

To test the membranes as a device, various solutions were prepared as electrolytes for the electrochemical measurements.

The electrolytes used on the electrochemical analysis were the following:

2.5.1 Glucose solution

Different concentrations of glucose solutions - 10 μM , 20 μM , 80 μM , 200 μM , 800 μM , 1 mM, 2 mM and 4 mM in water (pH: 5~7) - were evaluated. 5.5 mM and 7 mM were also prepared but ended being discarded. These concentrations were chosen based on the blood glucose levels of the human body, which are tightly correlated to sweat glucose levels and therefore, can be tested in a range to healthy from hypoglycemic. [31]-[33]

Glucose was purchased from Scharlab (D(+)-Glucose anhydrous, extra pure, Pharmapur®, pH Eur, BP, USP, $\text{C}_6\text{H}_{12}\text{O}_6$, Mw = 180.16 g/mol) and was used without further purification.

2.5.2 Glucose in NaOH

Different concentrations of Glucose solutions - 10 μM , 20 μM , 80 μM , 200 μM , 800 μM , 1 mM, 2 mM, and 4 mM in NaOH (pH 13) - were evaluated since glucose needs to be in a basic medium with high pH to guarantee oxidation [34], [35].

A glucose stock solution was used to prepare the more diluted solutions, such that a final concentration of 0.1 M NaOH was kept constant.

2.5.3 Artificial Sweat

Since body fluid pH is important to the patient's health, pH of solutions in the pH range of pH 4 – pH 8, was measured in artificial sweat solutions since the pH of human sweat is maintained in this region [36], [37].

L-Histidine ($C_6H_9N_3O_2$, Mw = 155.15g/mol, 99%(TLC) assay), Sodium Chloride (NaCl, Mw = 58.44g/mol, 99% assay), Sodium Phosphate Monobasic (NaH_2PO_4 , Mw = 119.98g/mol, 99% assay), Sodium Phosphate Dibasic (Na_2HPO_4 , Mw = 141.96g/mol, 99.95% assay) and Lactic Acid (Mw = 90 g/mol, 88% assay) all from Sigma Aldrich and used without further purification. Each component's concentration and percent of weight of solution in the solution's total volume is enumerated in Table 2.2 [38], [39]

Table 2.2 – Chemical composition of the three types of artificial sweat solutions used for the device's electrochemical measurements (adapted from [39])

	Concentrations (%(w/v))		
	AATCC (pH4)	ISO (pH6)	ISO (pH8)
Sodium Chloride	1.00	0.50	0.50
Lactic acid (88%)	0.097	-	-
L-Histidine	0.025	0.05	0.05
NaH_2PO_4	-	0.22	-
Na_2HPO_4	0.10	-	0.50

2.6 Electrochemical behaviour of the functionalized CA membranes with glucose and artificial sweat

All electrochemical measurements were carried out using a two-electrode electrochemical Teflon-made cell configuration, namely, a working electrode (WE) with a linearly varying potential through time, a platinum wire counter electrode (CE) to conduct electricity from the signal source to the WE and to serve as reference electrode (RE), to maintain a constant potential, and an electrolytic

solution, on a potentiostat (Gamry Instruments, Reference 3000). This configuration is better for systems with very low currents and short timescales, where the CE potential can be expected not to drift over the course of the experiment. Figure 2.5 shows a simple schematic of this configuration.

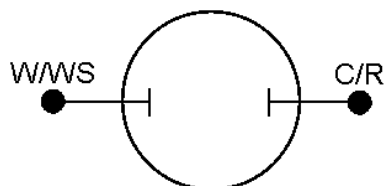


Figure 2.5 - Schematization of the chosen electrode configuration used in the electrochemical measurements, where W/WS represents the working electrode as well as the working sense and C/R represents the counter and reference electrode.

2.6.1 Cyclic Voltammetry

Cyclic voltammetry (CV) is an electrochemical technique used to evaluate redox behavior over a potential range at electrode surface, resulting in a voltammogram.

CV measures can generate oxidation states during the forward voltage scan and then reduce them on the reverse scan. The oxidation/reduction are function of the scan rates. [40].

For the electrochemical study of glucose and artificial sweat at the different functionalized membranes, three different electrodes were tested in a two-electrode configuration, schematized in Figure 2.6. Its characteristics are compiled in Table 2.3. Three different assemblages were tried out inside the Teflon-made cell - first, measurements were performed using each functionalized CA membrane as the WE, then the WE was replaced by a carbon strip on top of the membrane and finally, measurements were tried out using the carbon strip underneath the functionalized membranes as the WE. Only the last one was chosen as the default setting.



Figure 2.6 - Picture of the electrochemical Teflon-made cell used on the Cyclic Voltammetry studies.

Table 2.3 - Average sample thickness of the electrodes used in Cyclic Voltammetry that were scanned in both directions with 20, 40, 80 and 100 mV/s scan rates. Sample area: 1 cm².

Electrode Type	Average Sample Thickness (mm)
PANI/CA membrane	$(1.2 \pm 0.1) \times 10^{-1}$
PPy/CA membrane	$(1.4 \pm 0.02) \times 10^{-1}$
PEDOT/CA membrane	$(8.2 \pm 1.4) \times 10^{-2}$

All samples potential was scanned in both directions with different scan rates, namely: 20, 40, 80, 100 mV/s with 1 mL of six different electrolyte solutions: 0.1 M NaOH (pH 13), glucose, glucose in 0.1 M NaOH, AATCC (pH 4), ISO (pH 5) and ISO (pH 8) solutions. The glucose containing solutions were made with concentrations ranging from 10 μ M to 7 mM.

2.7 Amperometric detection of glucose and artificial sweat

2.7.1 Chronoamperometry

Chronoamperometry measures the current that goes through the electrochemical cell at a fixed potential as a function of time. A voltage is applied to the cell without a reaction occurring which is then stepped up by the addition of the analyte, initiating the electrode process, resulting in a current spike. Over the time, the current tends to drop off due to the material diffusion to the electrode surface for the reaction to happen.

All measurements were performed by applying an appropriate potential to the working electrode, studied previously by the cyclic voltammetry tests, to the two-electrode configuration cell.

Four different methodologies were tried out, thoroughly timed. The first method consisted in adding 1 mL of glucose electrolyte solution to the cell, then removing it. After the removal, 1 mL of Millipore® ultra-pure water was added, to wash the membrane, then removed. Next, a higher concentrated glucose electrolyte solution was added, removed, and the washing process was repeated. This was made continuously, on the same membrane, for concentrations ranging from 20 μM to 2 mM.

The second and third methods didn't involve membrane washing. They simply consisted in adding and removing, in a successive manner, to the same membrane, 1 mL of glucose solution. The only difference being that in the second method, glucose solution addition started from the lowest concentration (20 μM) to the higher concentrated ones and the third method went from highest to lowest concentrations.

Finally, the fourth method and the one adopted in all chronoamperometric measurements, was using different membranes for each electrolyte addition. Meaning that 1 mL of electrolyte was added and left stabilizing for a period of ten minutes. Then, the membrane was discarded.

Results and Discussion

In this section, the results obtained will be presented and discussed. First, the differently functionalized electrospun membranes' will be characterized using different techniques. Then, using glucose solutions with different concentrations and artificial sweat solutions with different pH values as electrolytes, the membranes electrochemical behaviour and their amperometric response was analysed.

3.1 Electrospun Membranes Characterization

All the electrospun cellulose acetate membranes functionalized with conductive polymers (PANI, PPy and PEDOT) by the methodology described in section 2.2 were analysed by SEM and ATR-FTIR.

Figure 3.1 shows SEM obtained images for CA electrospun membranes. The difference between them is that the CA electrospun membrane displayed in Figure 3.1(ii) was immersed in a 0.1M NaOH (pH 13) electrolyte for one hour.

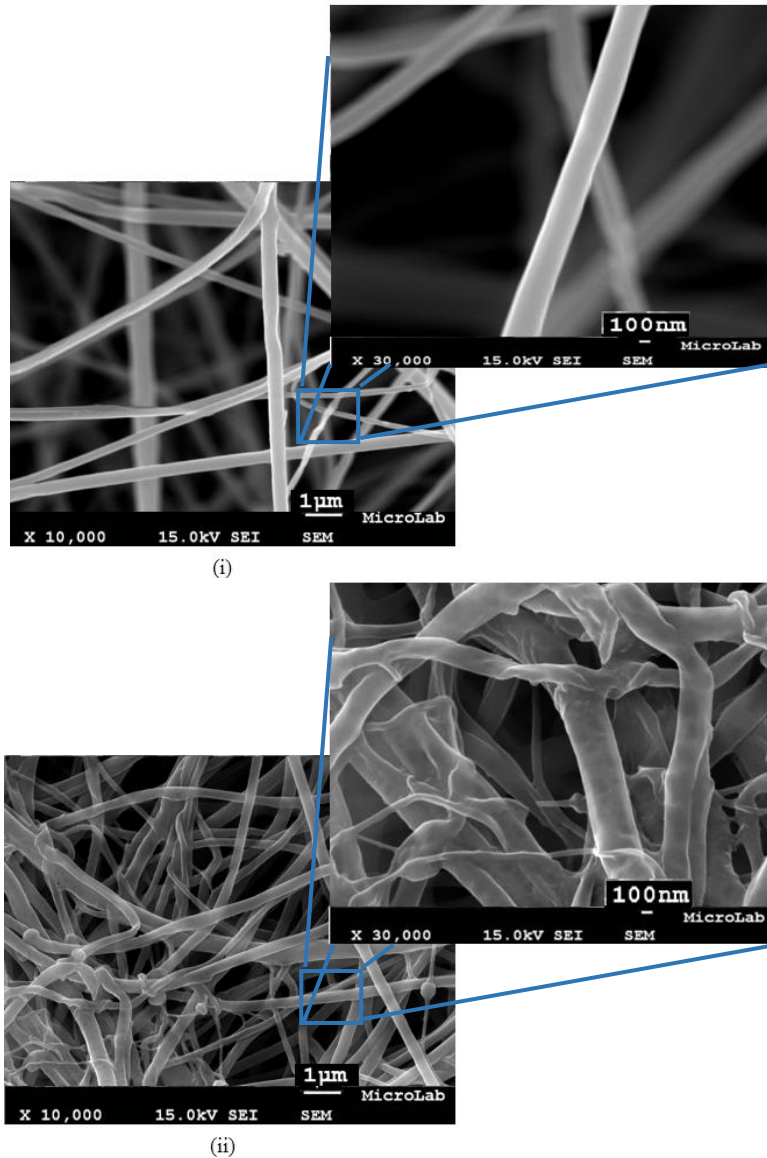


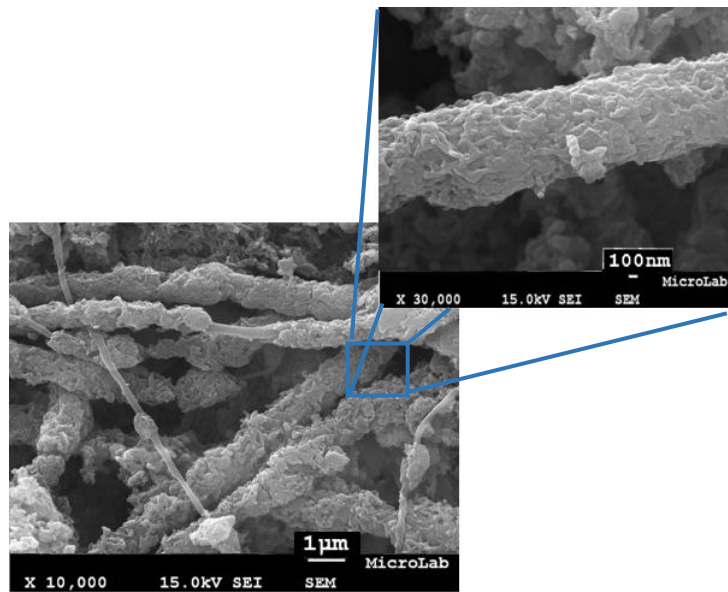
Figure 3.1 - SEM images of CA electrospun membrane (i) before and (ii) after immersion on a 0.1M NaOH (pH 13) electrolyte solution. Two different magnifications are displayed, x10000 and x30000

Since the membranes will be tested for different glucose concentrations like the ones found in healthy human blood and sweat, and glucose is easily oxidized in alkaline mediums, comparisons between the functionalized membranes performance towards acidic and basic pH values was previously performed.

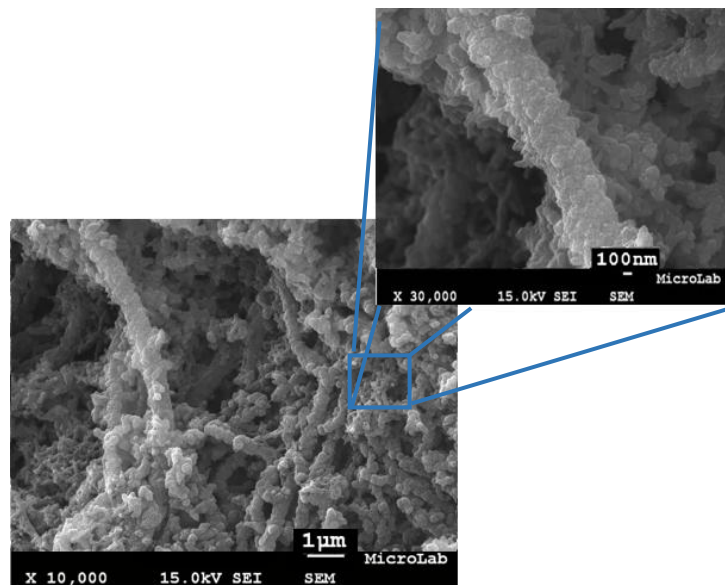
By immersing the membrane on a 0.1 M NaOH (pH 13) solution, it was possible to evaluate the behaviour of the conductive polymer functionalization

in a basic medium. The same was done with an acidic solution of HCl 0.1 M (pH 1), which completely degraded the membrane making it impossible to further test it.

An effective deposition of PANI on the fibers surface can be seen in Figure 3.2. A non-uniform coating of the fibers with the presence of PANI aggregates (Figure 3.2(i)) is noticed. The uniformity of the coating can be optimized by changing the polymerization time. Despite the polymerization time optimization done in a previous study [28], it is possible that fibers with a smaller diameter, or thinner fibers, are covered by an excess polyaniline while larger fibers are not, indicating that more polymerization time is needed.



(i)



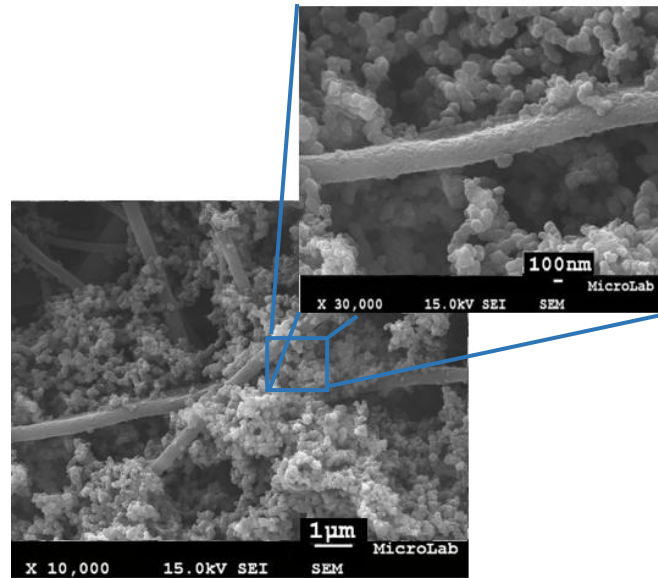
(ii)

Figure 3.2 – SEM images of CA electrospun membrane functionalized with PANI (i) before and (ii) after immersion on a 0.1M NaOH (pH 13) electrolyte solution. Two different magnifications are displayed, x10000 and x30000.

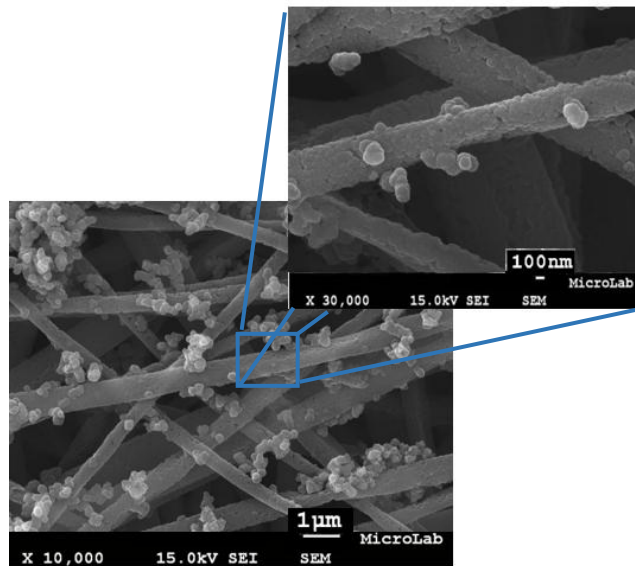
PANI functionalized CA membrane immersed in 0.1 NaOH solution (Figure 3.2(ii)) shows an apparent higher agglomeration of PEDOT outside fibers, whilst surface of fibers is getting more regular. Table 3.1 lists average fiber diameters.

The PANI layer presents an estimated thickness around the CA fibers of 52.4 ± 52 nm. Such high standard deviation is due to a rough estimate of the average diameter of fibers from SEM, since this is based on the difference between the CA fibers average diameter from Figure 3.1 and the PANI/CA average fiber diameter. In NaOH solution, is it clearly observed a fused web of electrospun fibers, with an increased thickness of 22% when compared to the non-immersed PANI layer.

PPy and PEDOT functionalized CA membranes' SEM imagens can be seen in Figures 3.3 and 3.4.



(i)



(ii)

Figure 3.3 - SEM images of CA electrospun membrane functionalized with PPy (i) before and (ii) after immersion on a 0.1 M NaOH (pH 13) electrolyte solution. Two different magnifications are displayed, x10000 and x30000.

The CA fibers are clearly covered by PPy (Figure 3.3(i)), although it is not uniform and PPy forms also a huge number of aggregates surrounding the fibers. The PPy layer covering the CA fibers has an estimated thickness of 40.4 ± 27 nm. When immersed in 0.1 NaOH solution, as shown in Figure 3.3(ii), most agglom-

erates disappear but CA fibers remain uniformly covered by PPy, being estimated a thickness increase by 25% in comparison with the non-immersed PPy layer.

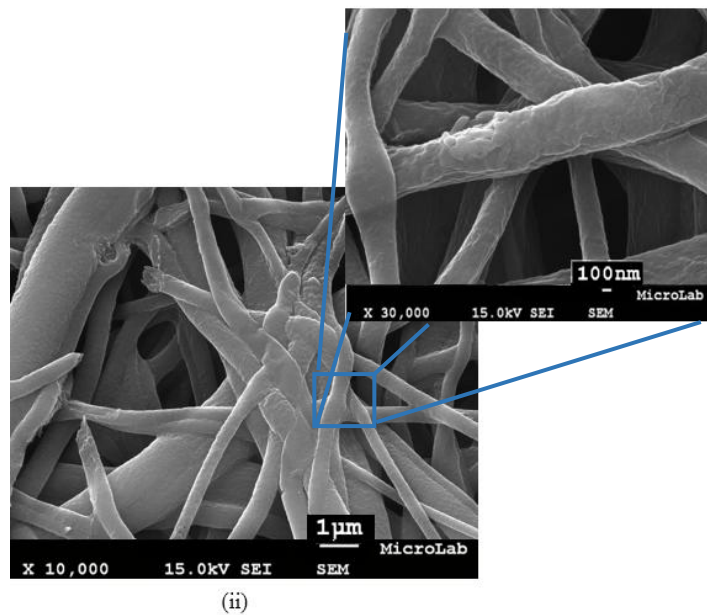
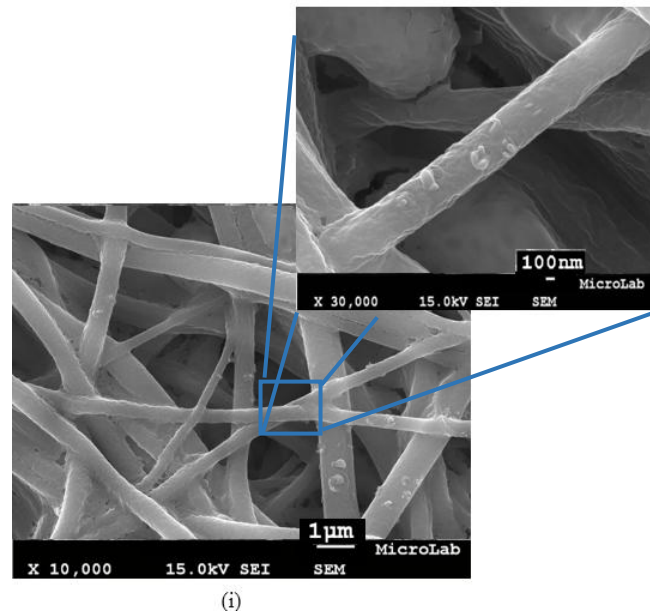


Figure 3.4 - SEM images of CA electrospun membrane functionalized with PEDOT (i) before and (ii) after immersed on a 0.1M NaOH (pH 13) electrolyte solution. Two different magnifications are displayed, x10000 and x30000

Figure 3.4 shows SEM images of CA membrane covered with PEDOT. A layer is covering the electrospun fibers surface with a thickness of $76\pm 38\text{nm}$ (Figure 3.4(i)). When immersed in 0.1 NaOH solution (Figure 3.4(ii)), brittle membrane may be caused by broken fibers seen in SEM images.

Table 3.1 - Average CA fiber diameters when functionalized with PANI, PPy and PEDOT before and after immersion in 0.1 M NaOH (pH 13) solution, 4 fibers were measured in each sample, 10 times each, using ImageJ® image processing software

	CA	PANI/CA	PPy/CA	PEDOT/CA
<i>D_{av} before electro-chemical characterization (nm)</i>	361.1±64	465.9±274	441.9±170	512.8±141
<i>D_{av} with 0.1 M NaOH electrolyte (nm)</i>	308.8±60	595.6±104	583.3±145	537.5±238

Average cellulose acetate fiber diameters increased after being functionalized, confirming that a conductive polymer layer was successfully deposited on the cellulose acetate matrix despite not being uniform.

ATR-FTIR was further performed to confirm the chemical composition of CA membranes functionalized with conductive polymers.

In Figure 3.5, the main infrared absorption bands of the polymers can be observed.

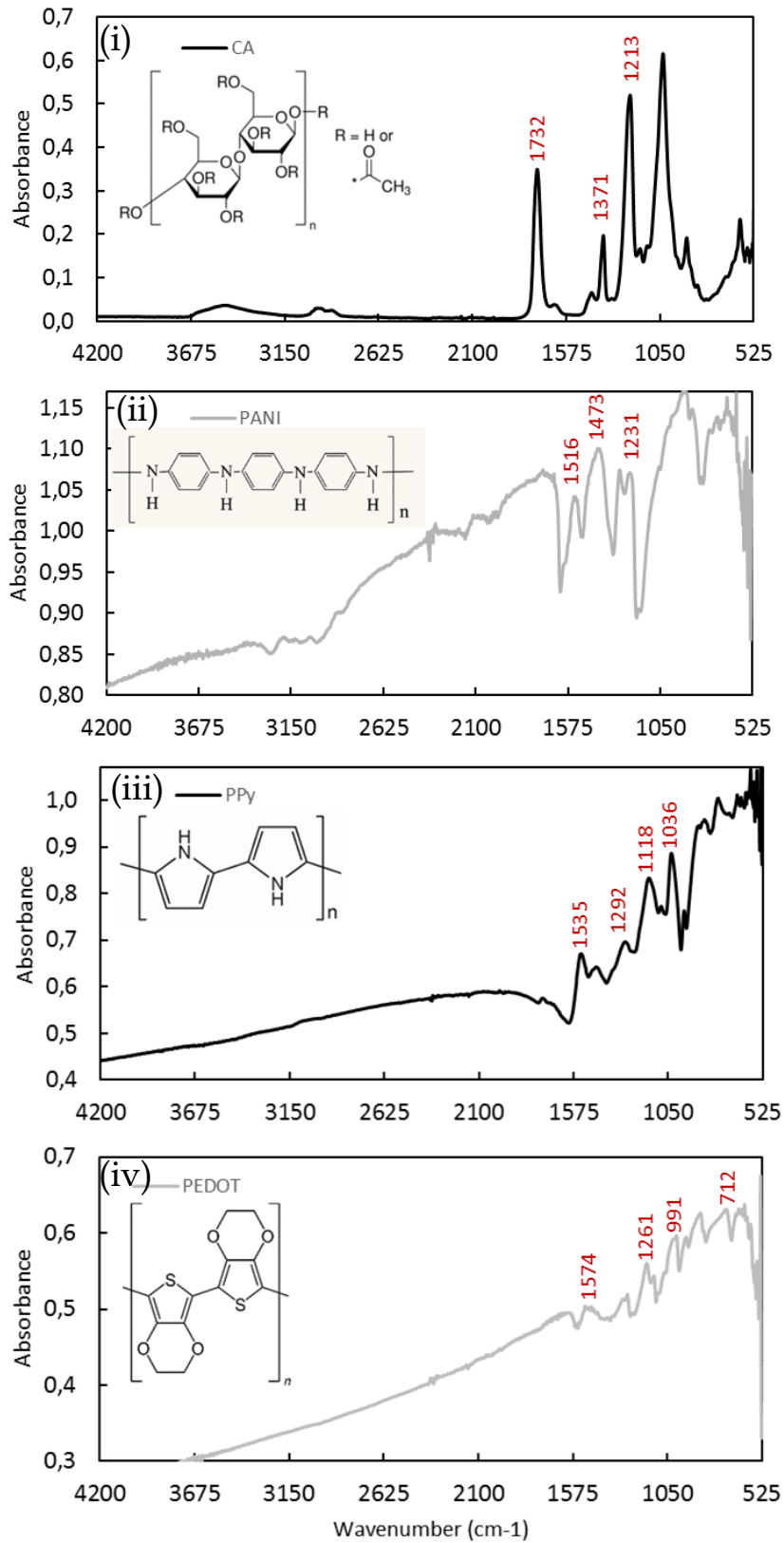


Figure 3.5 - ATR-FTIR spectra of CA (i), PANI functionalized CA (ii), PPy functionalized CA (iii) and PEDOT functionalized CA (iv) membranes.

Regarding CA spectra (Figure 3.5(i)), the absorption bands at 1732 cm^{-1} (C=O ester stretching) and 1371 cm^{-1} (CH) are assigned to the acetyl group on the polymeric chain, the last one being related to angular distortion in the ester methyl group. 1213 cm^{-1} band to C–O stretching of the acetyl group. The band present at 3439 cm^{-1} is allocated to the O–H stretching of the hydroxyl group [41], [42], [43].

Although there is a high absorption of the membranes in all wavenumber region due to its high thickness and dark colour, the finger-print of the FTIR peaks for each conductive polymer can be clearly observed. [44].

CA membrane functionalized with PANI spectra (Figure 3.5(ii)) shows absorbance values above 1, related to roughness of membranes. The absorption bands at 1516 cm^{-1} and 1473 cm^{-1} correspond to the quinone and benzene ring C = C stretches. The C–N stretch associated with 1273 cm^{-1} is visible as is the 1231 cm^{-1} band peak, assigned to the stretching mode of the protonated C–N group [45], [46].

ATR-FTIR absorption spectra of the PPy functionalized CA membrane (Figure 3.5(iii)) peaks at 1036 cm^{-1} and 1092 cm^{-1} can be assigned to C–H wagging. C–N stretch bonds are represented by the 1292 cm^{-1} band while C=N stretch corresponds to 1751 cm^{-1} . The characteristic peaks at 1535 and 1454 cm^{-1} associate to C=C stretching. The observed peaks confirm the presence of PPy in this membrane [37], [38].

As for the PEDOT functionalized CA membrane spectra (Figure 3.5(iv)), peaks at 1574 , 1446 and 1261 cm^{-1} can be assigned to the thiophene ring C=C and C–C stretch. The C–S bond can be seen at 991 , 858 and 712 cm^{-1} . Also, stretches of the ethylenedioxy group are at 1153 and 1082 cm^{-1} . 928 cm^{-1} representing the ethylene-dioxy ring deformation mode are observable [19].

Electrical conductivity of the successfully functionalized membranes was studied to understand the difference between each conductive polymer layer and to check the influence of immersion in 0.1 M NaOH solution.

As previously stated, electrical conductivity values of each different functionalized CA membrane were obtained from their corresponding I-V curves, in accordance to each sample's geometry, applying a potential from -1 to +1 V and measuring the corresponding electric current values. Figure 3.6 shows an example of one of the obtained I-V curves.

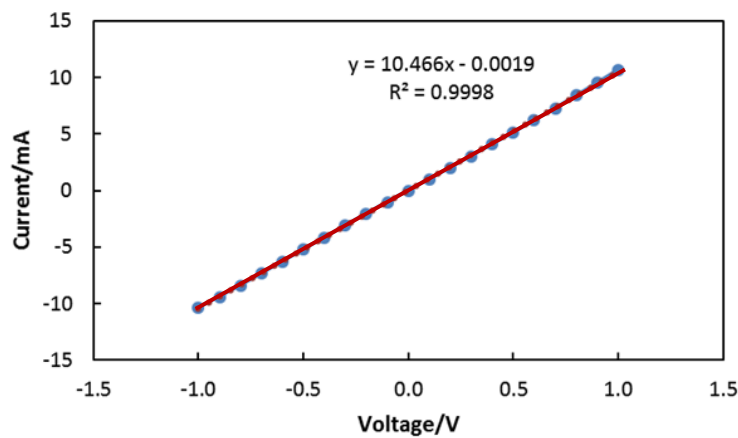


Figure 3.6 - Representative I-V Curve obtained for PEDOT/CA membrane.

Table 3.2 shows the conductivity values obtained for PANI/CA, PPy/CA and PEDOT/CA membranes, before (σ_{initial}) and after (σ_{final}) being immersed in 0.1 M NaOH solution, and corresponding membrane average thickness (T_{AV}).

The electrical conductivity of the membranes decreases when submitted to the basic medium which can be explained by the fact that conduction in these polymers is related with the degree of protonation which is dependant of pH. Thus, electronic conductivity becomes pH dependant and influenced by the anion's nature. The PEDOT/CA membrane inside basic mediums has therefore lower conductivity. [47], [48]

Table 3.2 - Conductivity of PANI/CA, PPy/CA and PEDOT/CA membranes, before (σ_{initial}) and after (σ_{final}) being dipped in 0.1 M NaOH solution, related to the corresponding membrane average thickness (T_{Av}).

	T_{Av} [mm]	σ_{initial} [S/cm]	σ_{final} [S/cm]
PANI/CA	$(1.2 \pm 0.1) \times 10^{-1}$	$(4.7 \pm 2.2) \times 10^{-3}$	$(2.6 \pm 0.05) \times 10^{-7}$
PPy/CA	$(1.4 \pm 0.02) \times 10^{-1}$	$(1.5 \pm 1.2) \times 10^{-1}$	$(2.4 \pm 0.3) \times 10^{-5}$
PEDOT/CA	$(8.2 \pm 1.4) \times 10^{-2}$	3.9 ± 1.2	$(1.3 \pm 0.001) \times 10^{-5}$

The PEDOT-functionalized CA membrane shows the best conductivity value (3.88 S/cm) when compared to PPy and PANI (Table 3.2). This result can be explained by the formation of a continuous and uniform PEDOT layer around the CA fibers (Figure 3.4(i)). However, the membrane's morphology is clearly affected after being immersed in a basic solution, as shown in Figure 3.4(ii) which may explain the decrease of conductivity value to 1.34×10^{-5} S/cm.

From the EIS measurements fitting it is obtained the hypothetical circuit parameters describing the membranes electrical behaviour.

PANI/CA example (Figure 3.7) emphasizes a blocking behaviour or the absence of a DC path through the circuit [49]. This mechanism can show inductive behaviour and can be schematized as the electrical circuit in Figure 3.8.

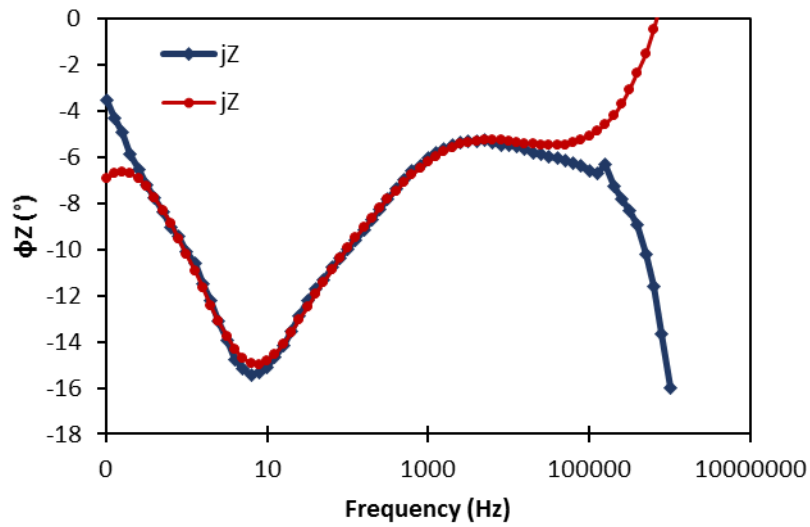


Figure 3.7 - EIS fitting curve of a PANI/CA membrane showing its current-voltage phase shift at low and high frequencies (red) and its EIS experimental curve (blue).

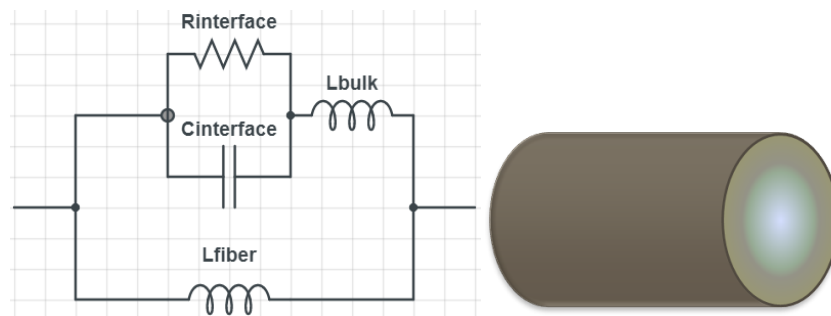


Figure 3.8 - Circuit model of a PANI/CA membrane showing the inductive behaviour of the fibers

Despite having a slight resistive behaviour at low frequencies, as the frequency raises, the inductive effect becomes clearer, meaning there is probably a non-covered inductive bulk of CA fibers.

PPy/equivalent electrical circuit of Figure 3.10 has been obtained after the fitting curve in Figure 3.9

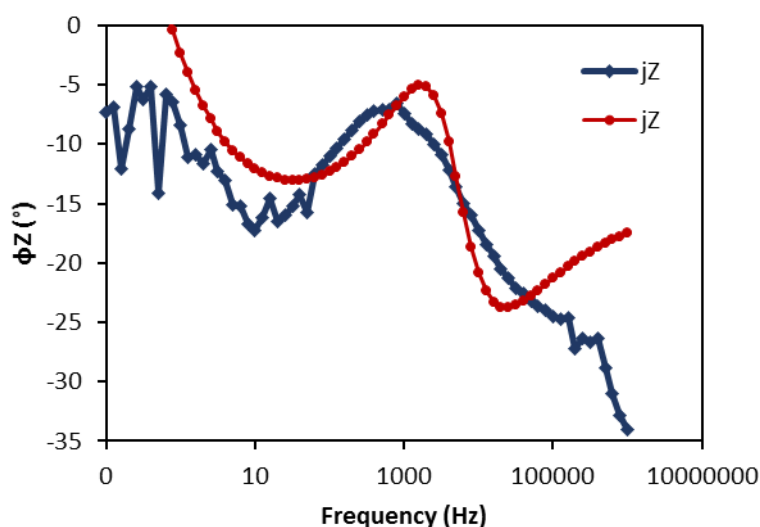


Figure 3.9 - EIS fitting curve of a PPy/CA membrane showing its current-voltage phase shift at low and high frequencies (red) and its EIS experimental curve (blue).

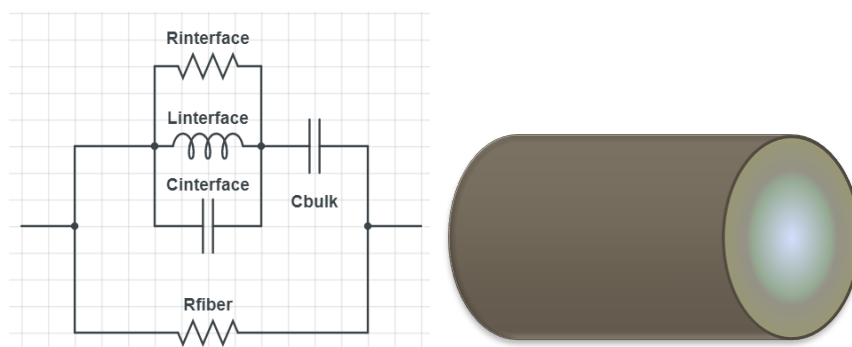


Figure 3.10 - Circuit model of a PPy/CA membrane at high frequency capacitance showing the non-covered insulating bulk of the CA fibers with PPy

The circuit model in Figure 3.10 reveals an inductive behaviour at low frequencies as well as a resistive character by looking at the wide range of frequencies that matches the membrane's interface. The charge carrier accumulation is due to capacitive interface and may be related to insulating fiber bulk.

PEDOT/CA shows two different cases. In the first case, the PEDOT/CA are highly conductive at DC. Following the EIS analysis, the wide range of frequencies show it has a resistive character (Figure 3.11). The current-voltage phase shift is close to zero, corresponding to a resistor. At high frequencies, a capacitive character is observed but non-prominent since there is a positive phase shift.

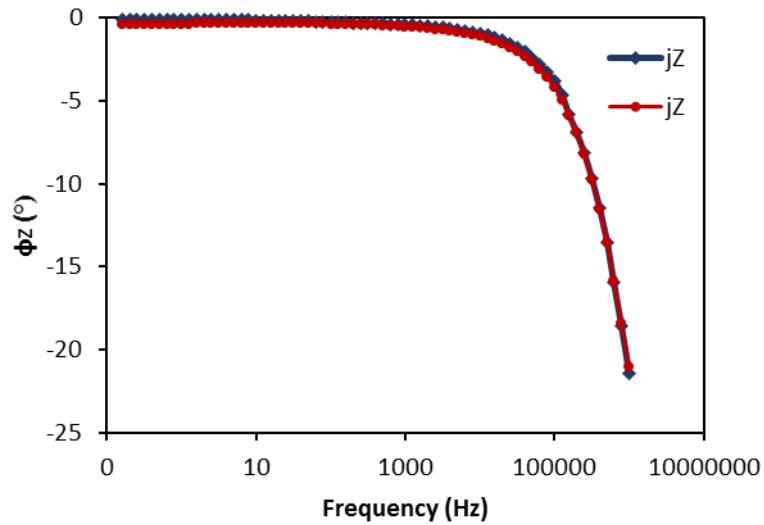


Figure 3.11 - EIS fitting of a PEDOT/CA membrane showing its current-voltage phase shift at low (zero) and high (positive) frequencies (red) and its EIS experimental curve.

Therefore, the model of the described PEDOT/CA membrane can be as shown in Figure 3.12, with a good fit, where the resistance of the fibers measuring is $R = 420 \Omega$ and the geometrical high frequency capacitance, is $C = 5 \text{ nF}$. It is then possible to assume that CA fibers are fully covered with PEDOT.

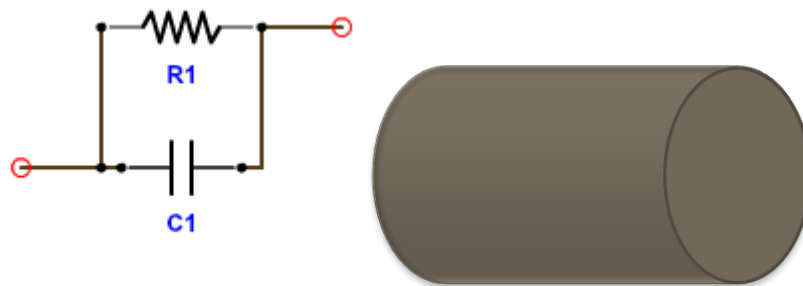


Figure 3.12 - Circuit model of a PEDOT/CA membrane at highly conductive DC showing the fully coverage of the CA fibers with PEDOT

The PEDOT/CA membrane has lower DC conductivity and the the EIS measurements' fitting is rather complicated (Figure 3.13).

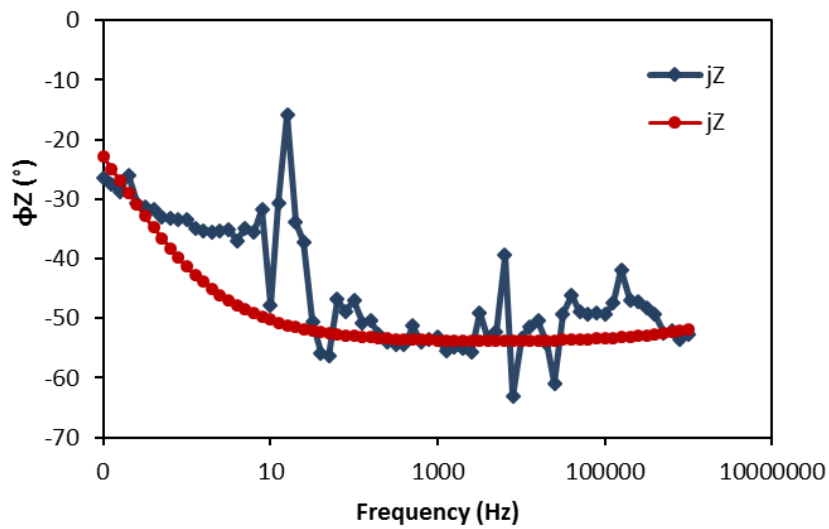


Figure 3.13 - EIS fitting of PEDOT/CA membrane showing its current-voltage phase shift at low and high frequencies (red) and its experimental curve (blue).

It can be seen, that the character of the membrane is rather capacitive, which means charge carrier accumulation. Thus, the equivalent circuit can be represented as it is in Figure 3.14.

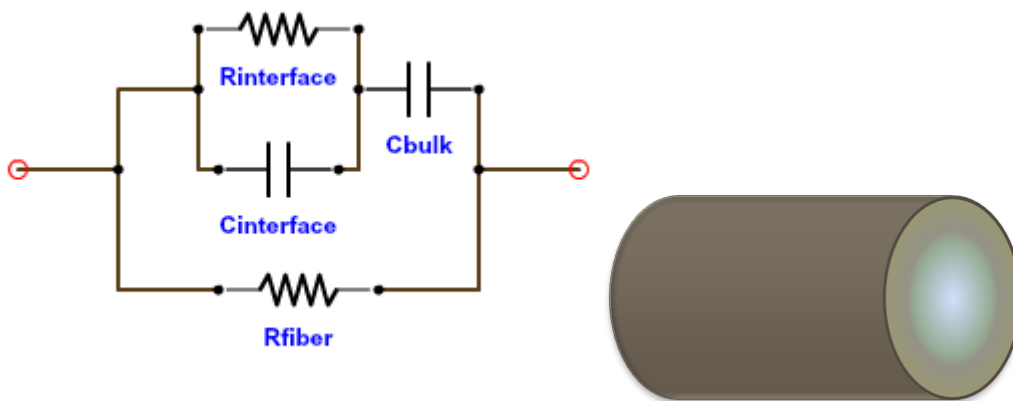


Figure 3.14 - Circuit model of a PEDOT/CA membrane at high frequency capacitance showing the non-covered insulating bulk of the CA fibers with PEDOT

In Figure 3.14 we observe parasitic geometrical high-frequency capacitance and a significant interfacial capacitance (2 nF). It is assumed that an uncovered insulating bulk of CA fibers acts as capacitor.

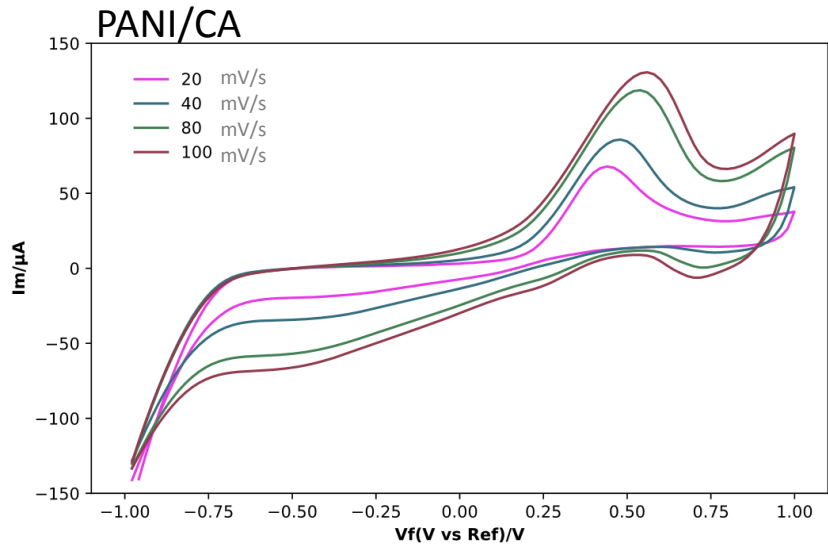
3.2 Electrochemical behaviour of glucose and artificial sweat at different electrodes

3.2.1 Cyclic Voltammetry

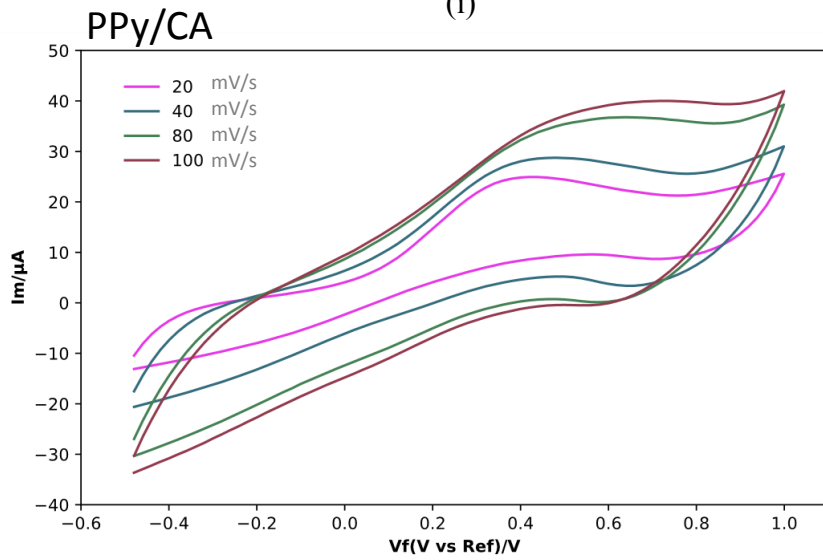
Cyclic Voltammetry was used to study the electrochemical behaviour of each of the conductive polymer functionalized membranes with different electrolytes. This way, the reduction and oxidation processes were assessed. Each measurement performed is destructive for the membrane, meaning that different set of CA functionalized membranes were used.

Despite trying different assemblages for the two-electrode configuration, only one prevailed, namely the one using the two electrode Teflon-made cell, with the platinum wire as the reference/counter electrode and the functionalized CA membrane with a carbon strip underneath as the working electrode. The comparative voltammograms of each assemblage can be seen on the Appendix, section A.1.

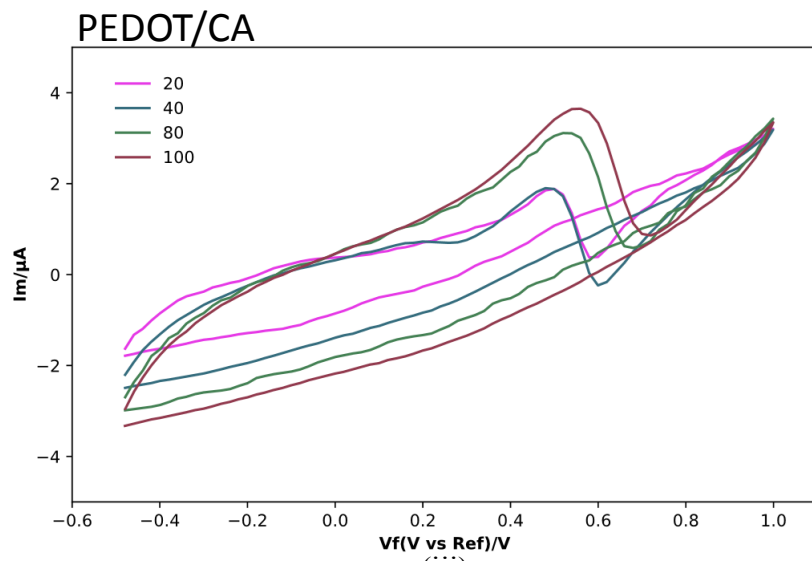
A study to determine the most suitable scan rate was performed using 1 ml solution of 0.1 M NaOH (pH 13) as the electrolyte. This electrolyte was tested since according to references [34] and [35], glucose needs to be in a basic medium with high pH to guarantee oxidation. PANI, PPy or PEDOT functionalized CA membranes were used as working electrodes with a carbon strip underneath to enhance electrical carriers collection. Cycle voltammetry was performed for scan rates in the range of 20 to 100 mV/s being tested 8 cycles. Figure 3.15 shows PANI, PPy and PEDOT cyclic voltammograms, using 1 ml electrolyte solution of 0.1 M NaOH, at 20, 40, 80 and 100 mV/s and an evaluation of the dependence of peak currents.



(i)



(ii)



(iii)

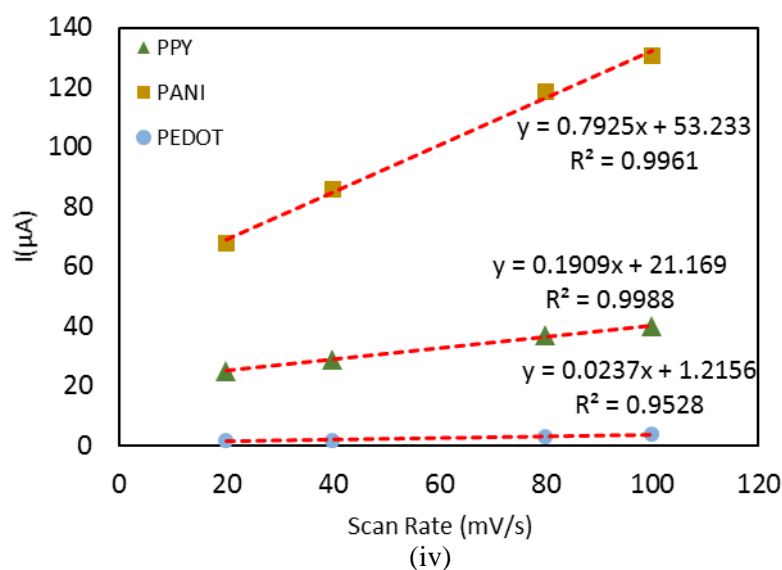
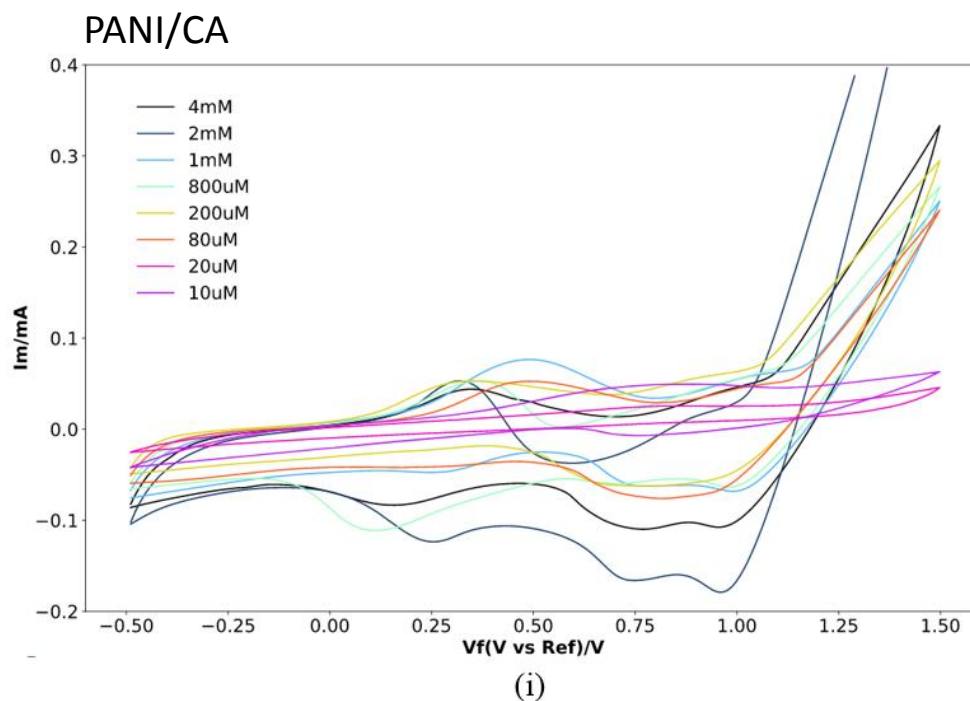


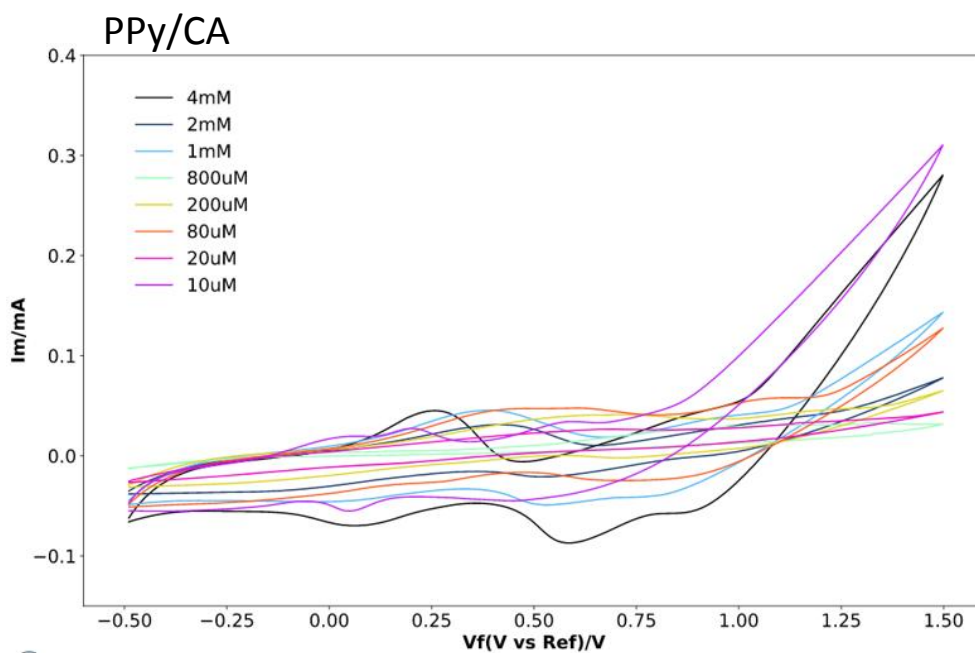
Figure 3.15 - PANI/CA (i), PPy/CA (ii) and PEDOT/CA (iii) voltammograms at 20, 40, 80 and 100 mV/s, for 8 cycles, with an applied potential between -1 to 1 V, only cycle 4 is presented and (iv) shows the dependence of the scan rate to PANI/CA, PPy/CA and PEDOT/CA's peak currents.

Each of the anodic peak shifted to more positive potentials, bestowing the kinetic limitation in the electrochemical reaction. Also, the anodic peak currents rise linearly with increasing scan rate, which proves that it is a surface-controlled electrochemical process [7], [50], [51]. Surface-controlled electrochemical processes are consequence of redox reactions at low scan rates on modified electrodes. At higher sweeps, the redox reactions start being controlled by diffusion processes [52]., for that reason, 80 mV/s was used as the preferred scan rate since the curves were the most well-defined ones and kept the surface-controlled process.

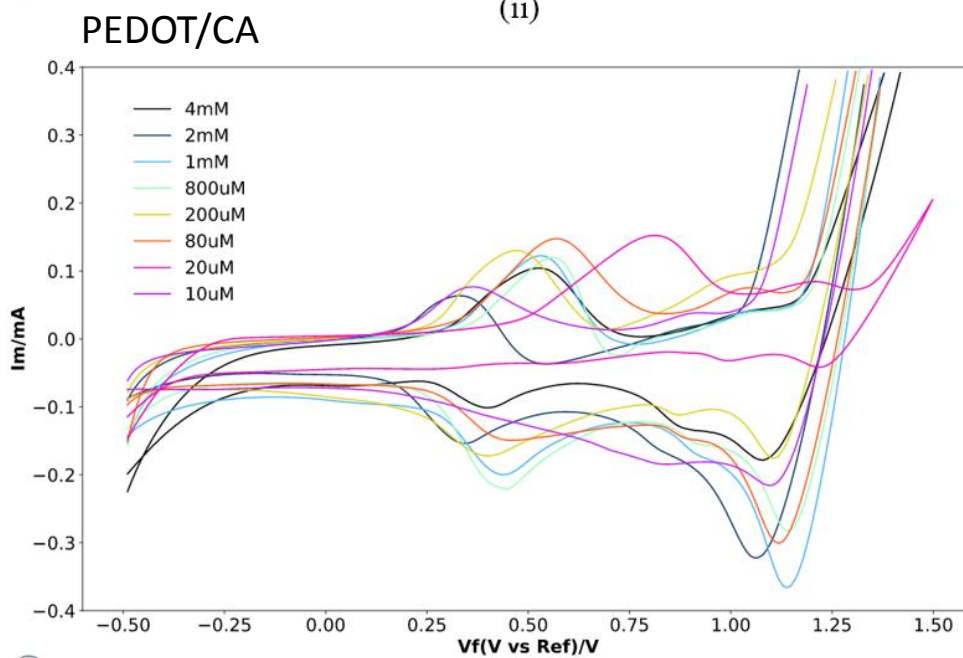
Selecting 80 mV/s scan rate, a cyclic voltammetric study of a new electrolyte was performed. Glucose solution (pH 6 ~ 7), with concentrations ranging from 10 μM to 4 mM. PANI and PEDOT electrodes showed anodic peaks, around +0.50 V and +0.20 V, respectively. Since glucose is not in an alkaline solution, the observed peaks belong to PANI and PEDOT [52]. PPy did not present peaks suggesting technical malfunctions during tests, namely short circuit, possibly due to contact between the platinum wire and the carbon strip. These results can be assessed in the Appendix, A.2.

As mentioned before, to guarantee the glucose's oxidation, 0.1 M NaOH solution (pH 13) was used. By doing so, the membrane material won't react. This time, glucose concentration was varied to match the sweat glucose concentration range [14], [53], [54]. Cyclic voltammograms responses obtained with ranging glucose concentrations from 10 μ M to 4 mM in such solution at a scan rate of 80 mV/s, in a total of 8 cycles, displaying curve 4, of PANI/CA, PPy/CA and PE-DOT/CA are shown in Figure 3.16. Applied potential ranged from -0.5 to +1.5 V. Glucose concentrations above 4 mM, namely 5.5 mM and 7mM were discarded since the electrode showed saturation and inconclusive results.





(ii)



(iii)

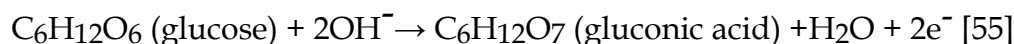
Figure 3.16 - PANI/CA (i), PPy/CA (ii) and PEDOT/CA (iii) voltammograms at 80 mV/s using different concentrations of glucose 0.1 M NaOH solution as electrolyte, for 8 cycles, with an applied potential between -0.5 to 1.5 V, only curve 4 is presented.

An analysis on each of the functionalized CA membrane voltammogram was performed. The peaks are compiled in Table 3.3.

Table 3.3 – Different concentrations of glucose 0.1 M NaOH solution and its corresponding functionalized membrane peak potentials

Glucose Concentration (mM)	PANI/CA		PPy/CA		PEDOT/CA	
	Peak Potential (V)	Peak Potential (V)	Peak Potential (V)	Peak Potential (V)	Peak Potential (V)	Peak Potential (V)
	Anodic	Cathodic	Anodic	Cathodic	Anodic	Cathodic
0.01	+0.89	+0.72	+0.07	+0.04	+0.37	+1.09
0.02	+0.84	+1.19	+0.70	+0.17	+0.82	+1.21
0.08	+0.50	+0.83	+0.49	+0.26	+0.58	+1.11
0.2	+0.36	+0.78	+0.72	+0.31	+0.48	+1.09
0.8	+0.38	+0.10	+0.00	+0.67	+0.57	+1.13
1	+0.50	+0.28	+0.40	+0.49	+0.54	+0.42
2	+0.33	+0.24	+0.43	+0.52	+0.34	+1.06
4	+0.36	+0.17	+0.27	+0.56	+0.54	+1.08

Glucose is a polyprotic acid with 5 OH groups. Keeping in mind that glucose is more acidic than alcohols with a pKa of about 12 ($K_a = 10^{-12}$), meaning the electronegative oxygen atoms in the molecule pull electron density away from the carbon atom bearing the negatively charged oxygen in the conjugate base, stabilizing it. The reaction mechanism of glucose in an alkaline medium is as follows:



Thus, the cyclic voltammograms in Figure 3.7, confirm that glucose is being oxidized.

It was expected to observe a linear dependency between the concentrations of the glucose solutions and their anodic peak current [7], [56], [57]. However, if the concentrations of glucose solutions are divided into two different groups (Group 1 – low concentration solutions – from 10 μ M to 200 μ M; Group 2

- high concentration solutions - from 800 μM to 4 mM) and the glucose concentration as a function of anodic peak current and potential as well as a function of cathodic peak current and potential are shown in Figure 3.17 for PANI/CA.

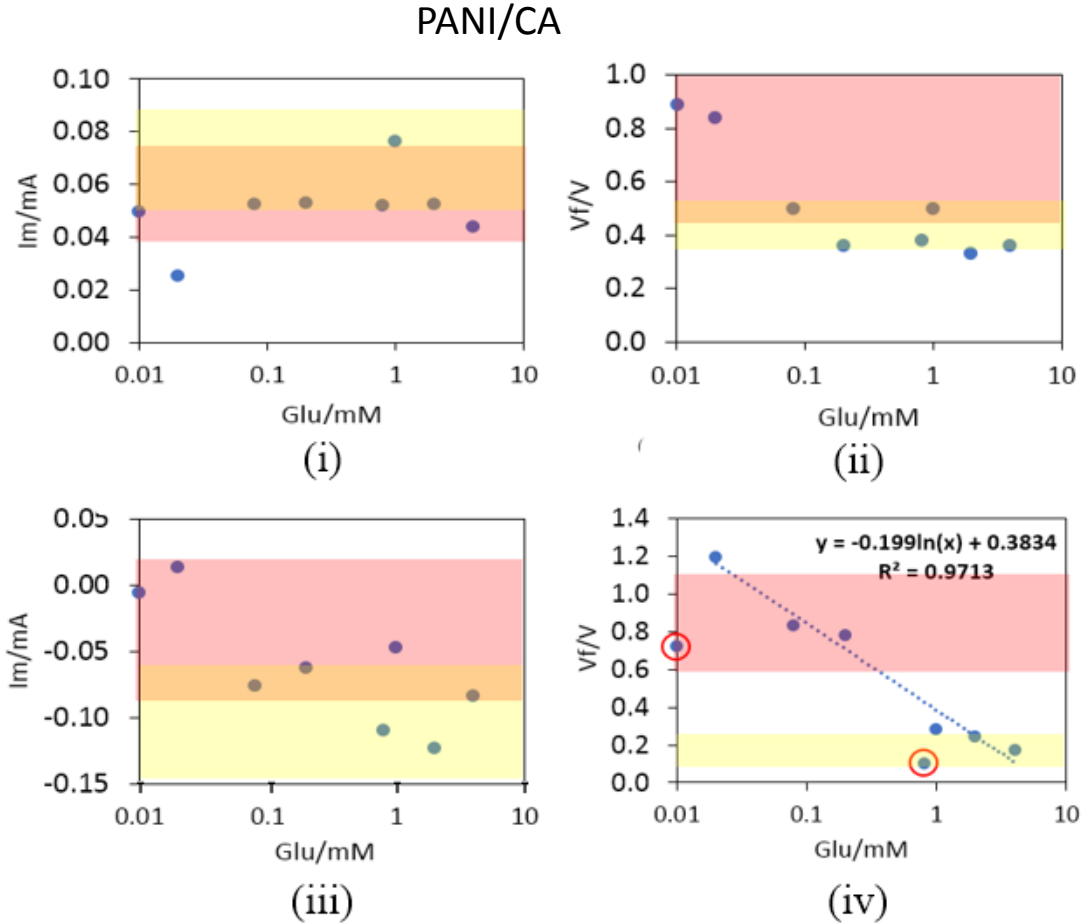


Figure 3.17 - Plots of glucose concentration versus anodic peak current (i), anodic peak potential (ii), cathodic peak current (iii), cathodic peak potential with a fitting done excluding data circled in red (iv), of the PANI/CA membranes. The coloured bars represent the standard deviation of the current or the potential. The red bars envelop the lower concentrations (10 μM , 20 μM , 80 μM , 200 μM) and the yellow bars envelop the higher concentrations (800 μM , 1mM, 2mM, 4mM).

Group 2 peak currents suggest membrane saturation, since they tend to stabilization. This might be because of the electrode area, which is too small and once immersed in group 2 solutions, beyond a certain threshold, could not produce more reaction. Group 1 peak currents might hint at some linear growth

when it comes to anodic and cathodic peak current but more intermediate glucose concentration solutions would be needed to test this possibility.

Regarding the fitting, in Figure 3.17(iv), to the cathodic peak potential values, 10 μM and 800 μM concentrations were left out, circled in red, hence a linear fitting was possible to attain. PANI/CA membranes may be sensitive to the two different ranges of glucose low and high concentrations.

PPy/CA relation as well as PEDOT/CA relation between glucose concentration and anodic and cathodic peaks are represented in Figures 3.18 and 3.19, respectively.

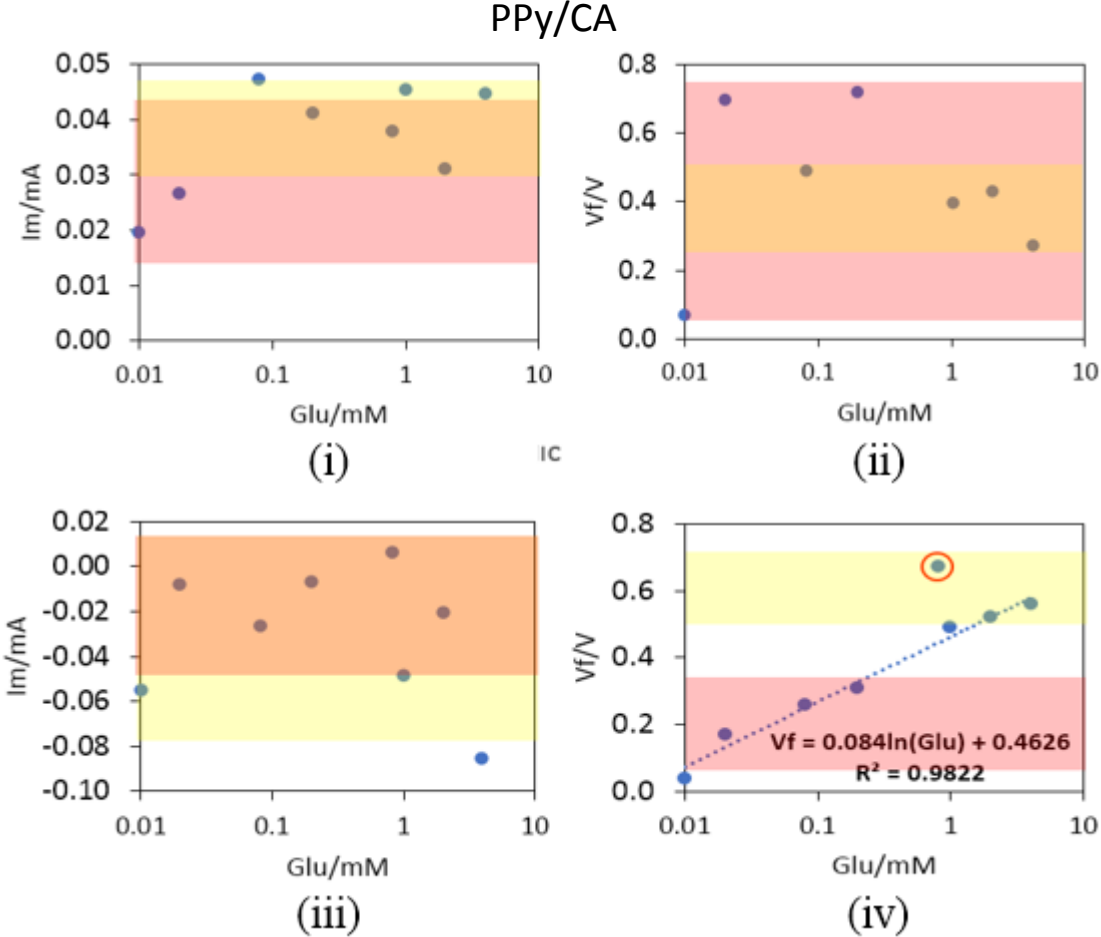


Figure 3.18 - Plots of glucose concentration versus anodic peak current (i), anodic peak potential (ii), cathodic peak current (iii), cathodic peak potential with a fitting done excluding data circled in red (iv), of the PPy/CA membranes. The coloured bars represent the standard deviation of the current or the potential. The red bars envelop the lower concentrations (10 μM , 20 μM , 80 μM , 200 μM) and the yellow bars envelop the higher concentrations (800 μM , 1mM, 2mM, 4mM).

PPy/CA cathodic peak potential grows linearly with the concentration of glucose, except for 800 μM glucose concentration, as can be seen in Figure 3.18 (iv). The coloured bars are also well separated, suggesting a clear distinction between the low glucose concentration regime and the higher concentration one. This means that PPy/CA is potentially sensitive to the distinct groups of different concentrations. The remainder relations of anodic peak current/potential and cathodic peak current with glucose concentration do not show a reliable correlation, as the bars are superimposed.

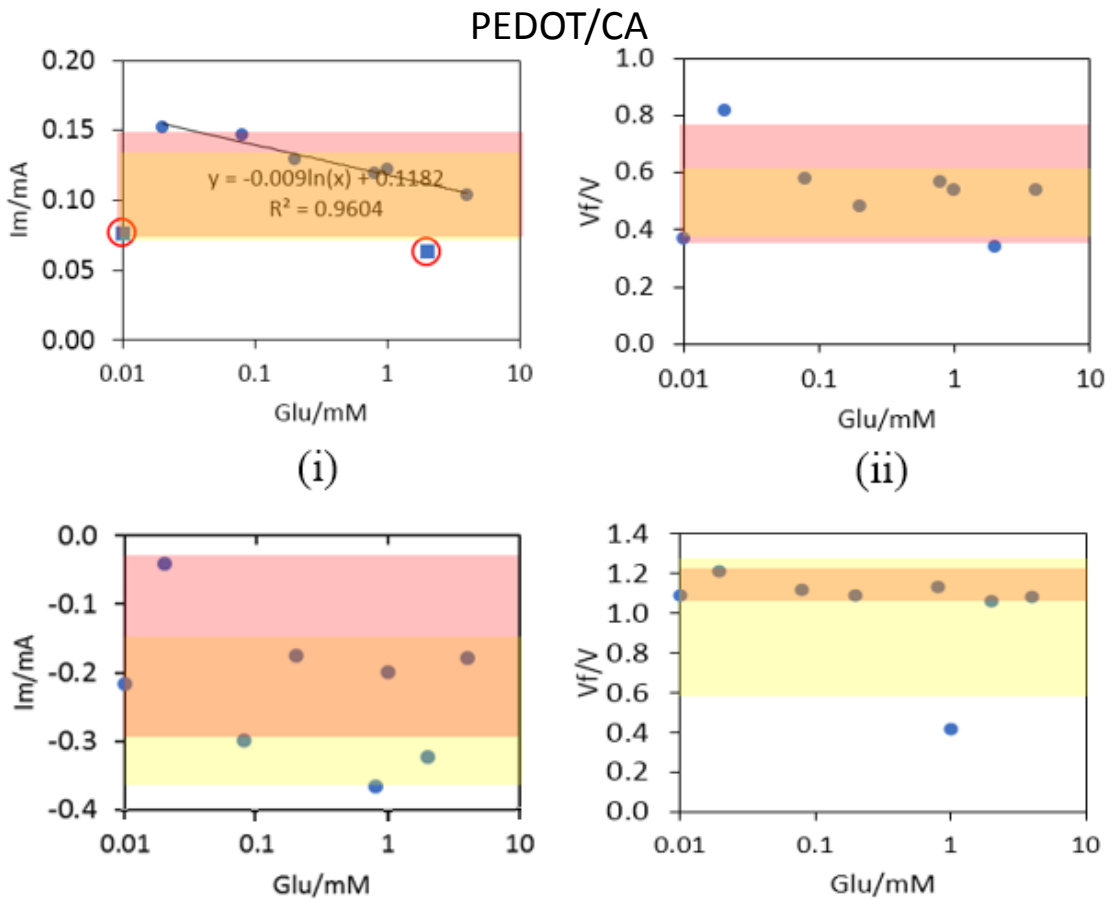


Figure 3.19 - Plots of glucose concentration versus anodic peak current with a fitting done excluding data circled in red (i), anodic peak potential (ii), cathodic peak current (iii), cathodic peak potential (iv), of the PEDOT/CA membranes. The coloured bars represent the standard deviation of the current or the potential. The red bars envelop the lower concentrations (10 μM , 20 μM , 80 μM , 200 μM) and the yellow bars envelop the higher concentrations (800 μM , 1mM, 2mM, 4mM).

PEDOT/CA anodic peak current relation shows a good fit when excluding 10 μ M and 2 mM, which means that this correlation may hint at this membrane's sensitivity to different glucose concentrations, while the other peak relations are not reliable.

Table 3.4 summarizes CV results obtained for glucose in 0.1 M NaOH listing the functional groups, correlation and coefficient of determination as well as corresponding peak where the fitting could be made, for each functionalized CA membrane.

Table 3.4 - Table summarizing PANI/CA, PPy/CA, PEDOT/CA functional groups, fitting equations, coefficients of determination and peak type

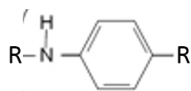
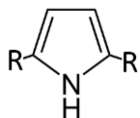
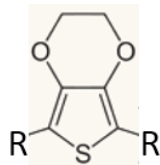
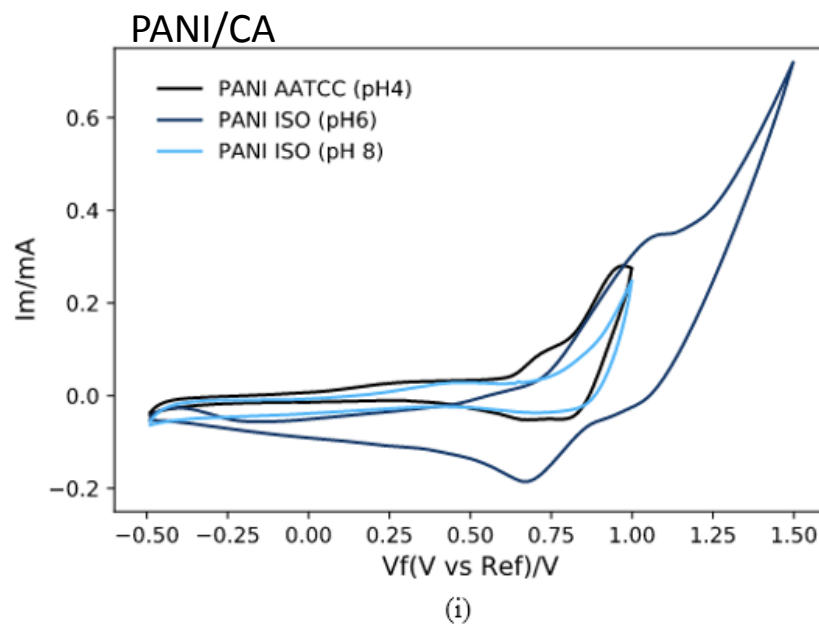
	Functional Group	Correlation	R²	Peak
PANI/CA		$V_f = -0.199 \ln(\text{Glu}) + 0.3834$	0.9713	Cathodic (Potential)
PPy/CA		$V_f = 0.084 \ln(\text{Glu}) + 0.4626$	0.9822	Cathodic (Potential)
PE-DOT/CA		$I_m = -0.009 \ln(\text{Glu}) + 0.1182$	0.9604	Anodic (Current)

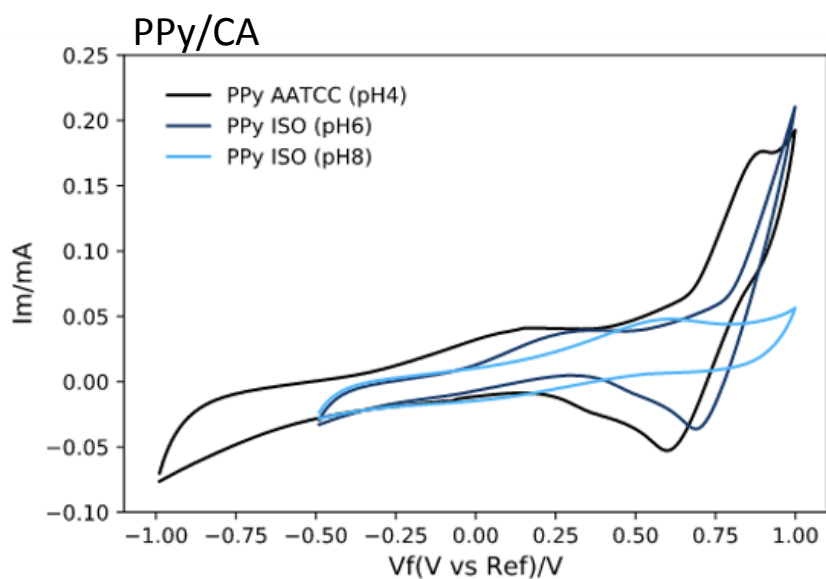
Table 3.6, shows a possible correlation between CA membranes functional group and the type of peak. For both PANI/CA and PPy/CA, the fitting of their respective cathodic peak potential may be a function of the amine group whereas for PEDOT/CA, that has a different functional group, namely the 3,4-ethylenedioxythiophene group, might be directly related to the anodic peak.

PANI/CA and PPy/CA have a correlation between the cathodic peak potentials and glucose concentration, meaning that the membranes are sensitive to gluconic acid, which is the oxidation product of glucose.

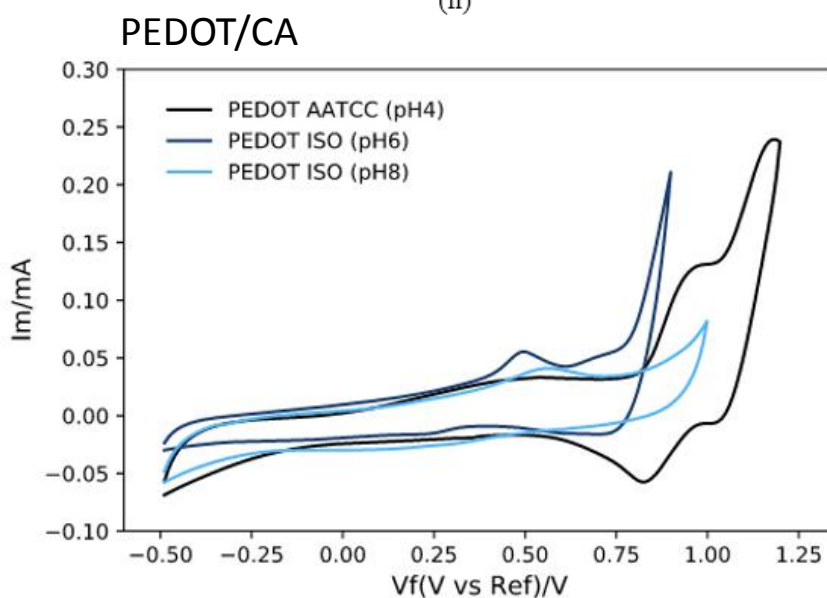
These results hint at the sensitive capacity of each functionalized membrane to different glucose concentrations.

The simulated sweat solutions studied in this project, namely AATCC (pH4), ISO (pH6) and ISO (pH8), cyclic voltammograms for PANI/CA, PPy/CA and PEDOT/CA using said electrolytes are displayed in Figure 3.8.





(ii)



(iii)

Figure 3.20 - Cyclic voltammograms for PANI/CA (i) for an applied range of potentials from -0.5 V to +1.5 V, PPy/CA (ii) for an applied range of potentials from -1.0 V to +1.0 V and PEDOT/CA (iii) for an applied range of potentials from -0.5 V to +1.2 V, all ran at 80 mV/s with three different artificial sweat simulating electrolytes with pH 4 (AATCC), pH 6 (ISO) and pH 8 (ISO). Curve 4 of 8 cycles in total is shown.

Figure 3.20(i) shows PANI/CA cyclic voltammograms with different artificial sweat simulating electrolytes. A study was first carried out to determine the more adequate applied potential: -0.5V to +1.0V. Peaks were observed for both

pH 4 and pH 8 but not for pH 6 (see Appendix A.3). The applied potential for pH 6 was then changed from -0.5V to +1.2V.

PANI/CA's anodic peak potential values (Figure 3.20(i)) were found at +0.76, +1.11 and +0.48V for pH 4, pH 6 and pH 8, respectively. This can be explained by the electrochemical behaviour of polyaniline when influenced by pH (Figure 3.21): at low pH levels, radical cations are formed and oxidized into imines afterwards showing oxidation above +0.65V, which means that at low concentration of protonic acid, both electron transfer and protonation peaks merge giving a usually broad peak at 0.40 V, which is consistent with the obtained results [47].

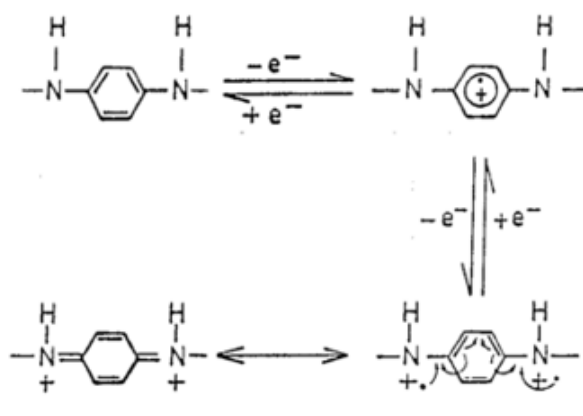


Figure 3.21 - Equation explaining PANI's electrochemical behaviour. Formation of radical cations leads to their oxidation into imines (adapted from [47]).

For PPY/CA, the applied potential of -0.5 to +1.0 V was adjusted to pH 4, to -1.0 to +1.0 V, since voltammograms do not show peaks (Appendix A.3). Anodic peak potential values were +0.89, +0.37 and +0.61 V for pH 4, pH 6 and pH 8, respectively. PPy growth is inhibited at pH 7 but the increase of anodic current reveal that oxidation of oligomers initially is easier than the monomers. When oxidizing, pyrrole rings form carbonyl groups and consequently lose its conjugation (Figure 3.22).

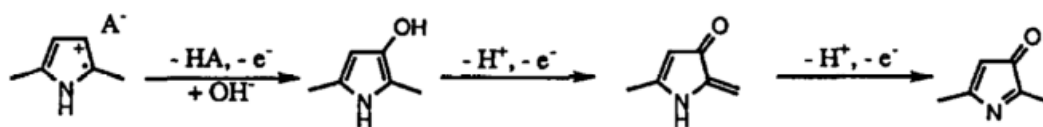


Figure 3.22 – Scheme representing the oxidation of pyrrole rings and their loss of conjugation when the forming of carbonyl groups occur [48].

PEDOT/CA in Figure 3.20(iii) needed applied potential adjustment for pH 4 (-0.5 to +1.2V) in order to make the anodic peak curve value clearer (trial using -0.5 to +1.0V can be seen in Appendix A.3). For pH 6 and pH 8, applied potentials used were -0.5 to +1.0V. Anodic peak values of +0.89, +0.37 and +0.61V were obtained respectively for pH 4, 6 and 8. This variation can be explained by the fact that oxygen attached to the β -position of the thiophene ring supports the delocalization of positive charges on the PEDOT backbone [48].

3.3 Amperometric detection of glucose and artificial sweat

3.3.1 Chronoamperometry

To improve the performance of the PANI, PPy and PEDOT functionalized CA membranes as a biosensor, the effects of pH and the detection potential on the current response should be optimized to enhance sensitivity. The amperometric response depends on the applied potential.

The effect of the applied potential on the electrochemical oxidation of glucose was studied previously (Section 3.2). By increasing the applied potential in order to match the electrochemical oxidation peaks of glucose, the current increases, meaning that the electrode's response results from the electrochemical oxidation of glucose [51], [57]. To a higher than +0.7 V applied potential, the response current starts to level off, so the selected potential for glucose and for the different pH artificial sweat detection was +0.6 V [57].

The amperometric response was recorded with 1 mL glucose solution in concentrations ranging from 10 μ M to 2 mM and with 1 mL artificial sweat solutions with pH values ranging from 4 to 8, on the PANI, PPy and PEDOT electrodes, during a stabilizing period of 10 minutes. The chosen methodology was

the one stated in Section 2.7.1, that comprised using different membranes for each electrolyte addition, whose results can be seen in Figure 3.23 and 3.24. The other methodologies results can be accessed in Appendix A.4.

In Figure 3.23 (i), glucose concentration of 2 mM of the PANI/CA membrane had to be left out since the output corresponded to a technical malfunction, namely, short circuit. As can be seen, shortly after the addition of glucose solution, the oxidation current increases and reaches a steady state within approximately 200 s.

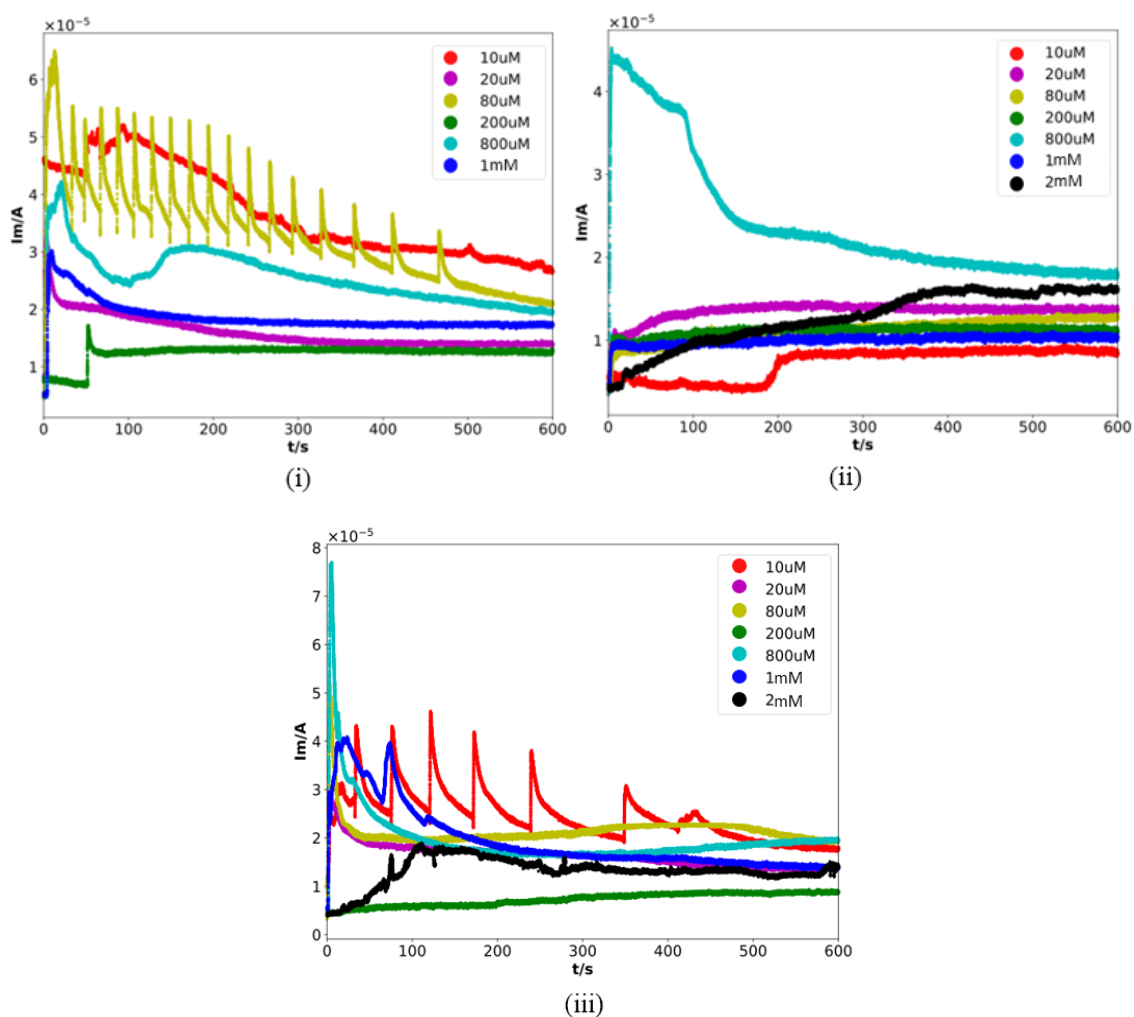


Figure 3.23 – Chronoamperograms of PANI/CA (i), PPy/CA (ii) and PEDOT/CA (iii) for different glucose concentrations ranging from 10 μ M to 2 mM using an applied potential of +0.6 V

The results in Figure 3.23 are rather inconclusive since the applied potential was not the appropriate one. A different potential should have been applied to each different functionalized membrane, comprising the cathodic peak potentials, which admitted correlation in both PANI/CA and PPy/CA cases, within a specific range for both low and high concentration glucose solutions.

Amperometric response of artificial sweat solutions is shown in Figure 3.24 whereas its stabilization current values (in μA) are listed on Table 3.5.

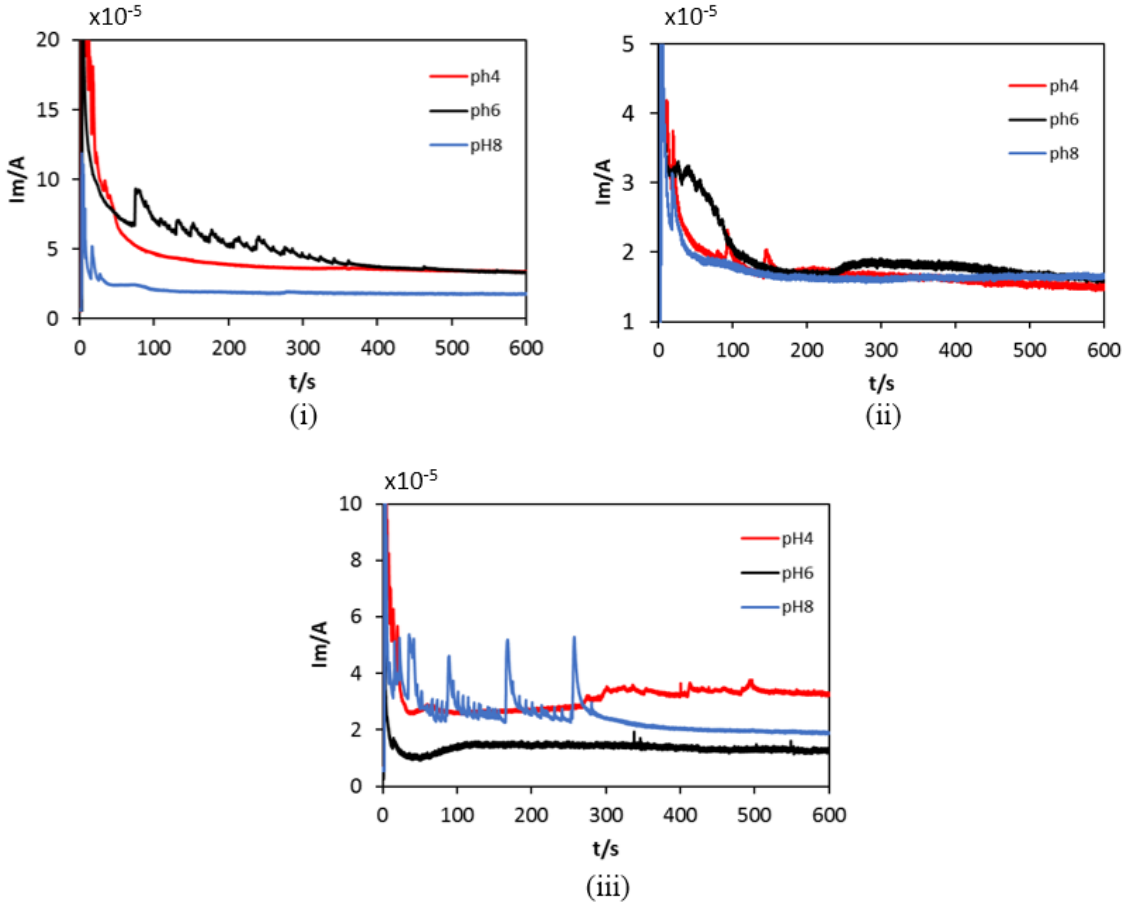


Figure 3.24 - Chronoamperograms of PANI/CA (i), PPy/CA (ii) and PEDOT/CA (iii) for different artificial sweat solutions at pH ranging from 4 to 8, using an applied potential of +0.6 V

Tabela 3.5 – Table comprising the stabilization current in μA taken from the chronoamperograms for PANI/CA, PPy/CA and PEDOT/CA, as function of different artificial sweat solution pH, namely, pH4, pH6 and pH8, for a time period of 300 s, approximately.

<i>pH</i>	<i>Current (μA)</i>		
	<i>PANI/CA</i>	<i>PPy/CA</i>	<i>PEDOT/CA</i>
4	34.7	15.6	33.4
6	29.8	20.1	10.3
8	18.2	16.2	20.8

By looking at the chronoamperograms in Figure 3.24, during the instant moment ($t \approx 0$ s) of the electrolyte addition to the cell, a current peak occurs. This peak is product of the immersion of the platinum reference electrode and not necessarily from the working electrode immersion with the electrolyte. The current then decreases towards stabilized values ($t \approx 300$ s). Those values are listed in Table 3.4. Since only three different pH values were tested, there is not enough data to establish a valid correlation. Adjusting the pH of the used artificial sweat solutions with NaOH and HCl solutions would be a way to overcome such limitation and provide more information.

4

Conclusions

This chapter presents the main results and conclusions of this work. Future perspectives for new developments and ways to integrate the developed membranes are also suggested.

4.1 - General Conclusions

Present work's initial proposed aims were met. An electrospun cellulose acetate membrane with multisensorial characteristics was developed.

Polymeric fibers of cellulose acetate were produced by electrospinning technique using previously studied optimized conditions from previous works. The obtained fibers were functionalized either with polyaniline by *in situ* oxidation of Aniline in aqueous solution, with polypyrrole by *in situ* oxidation of Pyrrole in aqueous solution or with PEDOT by vapor-phase polymerization of EDOT. The produced functionalized membranes were then characterized.

SEM technique was used to characterize the fibers morphology before and after immersing the membranes in an alkaline medium - a 0.1 M NaOH solution. It was possible to conclude that there was a uniform conductive polymer deposition along the cellulose acetate fibers, whose diameter increased after immersion in 0.1 M NaOH solution. ATR-FTIR proved there was interaction between CA and the conductive polymers. The peaks observed on the different conductive polymer functionalized CA membranes matched with the ones found in the

literature despite positional fluctuation of peaks that could be due to masking by other elements.

Electrical conductivity values for each different functionalized CA membrane were obtained from their corresponding I-V curves, in accordance to each sample's geometry. When submitted to the basic medium, it drastically decreased which can be explained by the fact that conduction in these polymers involves protonation and access to counterion in order to keep charge neutrality. EIS measurements fittings were obtained to describe the membranes behaviour as electrical circuits. All PANI/CA, PPy/CA hinted at non-covered insulated fiber bulk due to charge accumulation, justifying their low conductivity. One PEDOT/CA sample model corresponded to a fully covered fiber.

Cyclic Voltammetry was used to study the electrochemical behaviour of each of the conductive polymer functionalized membranes with different electrolytes. After deciding on a suitable 80 mV/s scan-rate using 0.1 M NaOH (pH 13) as the electrolyte to guarantee glucose oxidation, cyclic voltammetry was performed on the CA functionalized membranes using different concentrations of glucose in a glucose water solution and in a glucose 0.1 M NaOH solution. An analysis of the glucose concentration as a function of anodic peak current and potential was possible as well as a function of cathodic peak current and potential for different glucose concentrations on 0.1 M NaOH. There was a correlation between the functionalized CA membranes functional group and the type of peak in the voltammogram. For both PANI/CA and PPy/CA, the fitting of their respective cathodic peak potential could be a function of the amine group whereas for PEDOT/CA, the anodic peak current could be directly related to 3,4-ethylenedioxythiophene group.

PANI/CA and PPy/CA membranes may be sensitive to gluconic acid, which is the oxidation product of glucose and PEDOT/CA membranes can be sensitive to glucose by its interaction with its functional group. Thus, there is a sensitive capacity of each functionalized membrane to different glucose concentrations. This could be further certified by replicating results with more samples in future works.

Functionalized CA membranes are also sensitive to pH. Using the artificial sweat solutions with different pH and studying its anodic peak potentials, results

matched those found in literature. PANI/CA's anodic peak potential +0.76, +1.11 and +0.48V for pH 4, pH 6 and pH 8. For low pH levels, radical cations oxidize into imines, producing peaks above +0.65V, therefore, at low concentration of protonic acid, both electron transfer and protonation peaks merge giving a usually broad peak at 0.40 V. Regarding PPy/CA, anodic peak potentials were +0.89, +0.37 and +0.61V for pH 4, pH 6 and pH 8, respectively. Since PPy growth is inhibited at pH 7, the anodic current shift was due to the oligomers initially produced oxidation. Pyrrole rings form carbonyl groups and consequently lose its conjugation when oxidizing. For PEDOT/CA, anodic peak values were +0.89, +0.37 and +0.61V for pH 4, 6 and 8. Increasing pH suggests loss of activity but PEDOT tends towards stabilization because the Oxygen attached to the β -position of the thiophene ring supports the delocalization of positive charges on the polymer backbone.

Regarding different concentrations of glucose, chronoamperometric response was deemed inconclusive as the applied potential was not the most appropriate one. A different potential should have been applied to each different functionalized membrane, comprising the cathodic peak potentials, which admitted correlation in both PANI/CA and PPy/CA cases, within a specific range for both low and high concentration glucose solutions, as well as the PEDOT/CA anodic peak potential values.

Artificial sweat chronoamperograms revealed that current lowered to steady-like values after a period of approximately 300 s. Since only three different pH values were tested, there was not enough data to establish a valid correlation between pH values and stabilizing current values. Adjusting the pH of the used artificial sweat solutions with NaOH and HCl solutions would be a way to overcome such limitation and provide more information, since that way, artificial sweat solutions could have intermediate pH values.

4.2 - Final Thoughts

This project meant to test possible electrodes to serve as components of a more complete device. Nowadays' researchers are beginning to envision and develop sensors that use microfluidics as artificial skin, biosensing tattoos and MEMS-made patches. This membrane offers the possibility to be included in such sensors to improve healthcare.

Since turning patient care and diagnosis more accessible and convenient is one of today's researching priorities, incorporating green chemistry, inexpensive materials and minimal size while using non-invasive testing methods was the basis for this membrane development.

To conclude, it is pertinent to reiterate that the obtained results represent a definite direction for research in glucose and pH biosensors for clinical purposes using electrospun CA membranes functionalized with PANI, PPy and PEDOT. Even though further testing is still necessary, its discussion leads towards new research direction.



Bibliography

- [1] J. Wang, "Glucose Biosensors : 40 Years of Advances and Challenges," *Electroanalysis*, vol. 1312, pp. 983–988, 2001.
- [2] B. D. Malhotra and A. Chaubey, "Biosensors for clinical diagnostics industry," *Sensors Actuators, B Chem.*, vol. 91, no. 1–3, pp. 117–127, 2003.
- [3] E.-H. Yoo and S.-Y. Lee, "Glucose Biosensors: An Overview of Use in Clinical Practice," *Sensors*, vol. 10, pp. 4558–4576, 2010.
- [4] D. O'Hare, "Biosensors and Sensor Systems BT - Body Sensor Networks," G.-Z. Yang, Ed. London: Springer London, 2014, pp. 55–115.
- [5] M. Gerard, A. Chaubey, and B. D. Malhotra, "Application of conducting polymers to biosensors," *Biosens. Bioelectron.*, vol. 17, no. 5, pp. 345–359, 2002.
- [6] A. C. R. Grayson *et al.*, "A BioMEMS review: MEMS technology for physiologically integrated devices," *Proc. IEEE*, vol. 92, no. 1, pp. 6–21, 2004.
- [7] B. Zheng *et al.*, "A sensitive AgNPs/CuO nanofibers non-enzymatic glucose sensor based on electrospinning technology," *Sensors Actuators, B Chem.*, vol. 195, pp. 431–438, 2014.
- [8] D. Bruen, C. Delaney, L. Florea, and D. Diamond, "Glucose Sensing for Diabetes Monitoring: Recent Developments," *Sensors*, vol. 17, no. 8, p. 1866, 2017.
- [9] X. Chen, G. Wu, Z. Cai, M. Oyama, and X. Chen, "Advances in enzyme-free electrochemical sensors for hydrogen peroxide, glucose, and uric acid," *Microchim. Acta*, vol. 181, no. 7–8, pp. 689–705, 2014.
- [10] S. Park, H. Boo, and T. D. Chung, "Electrochemical non-enzymatic glucose

- sensors," *Anal. Chim. Acta*, vol. 556, no. 1, pp. 46–57, 2006.
- [11] Á M. T., B R. D., and S. J. C, "Flexible Electronic Skin," vol. 4, no. 6, pp. 4041–4046, 2014.
- [12] D. Figeys and D. Pinto, "Lab-on-a-Chip: A Revolution in Biological and Medical Sciences," *Anal. Chem.*, vol. 72, no. 9, p. 330 A-335 A, 2000.
- [13] M. Meyer, N. Van Binh, V. Calero, L. Baraban, J. Rogers, and G. Cuniberti, "A Stretchable and Flexible Platform for Epidermal Electronics," *Adv. Sci. Technol.*, vol. 102, pp. 65–67, 2016.
- [14] H. Lee *et al.*, "Wearable/disposable sweat-based glucose monitoring device with multistage transdermal drug delivery module," *Sci. Adv.*, vol. 3, no. 3, p. e1601314, 2017.
- [15] I. Ferreira, B. Brás, N. Correia, P. Barquinha, E. Fortunato, and R. Martins, "Self-Rechargeable Paper Thin-Film Batteries: Performance and Applications," vol. 6, no. 8, pp. 332–335, 2010.
- [16] A. Baptista, I. Ferreira, and J. Borges, "Cellulose-Based Bioelectronic Devices," *Cellul. - Medical, Pharm. Electron. Appl.*, pp. 67–82, 2013.
- [17] W. Amass, A. Amass, and B. Tighe, "A review of biodegradable polymers: uses, current developments in the synthesis and characterization of biodegradable polyesters, blends of biodegradable polymers and recent advances in biodegradation studies," *Polym. Int.*, vol. 47, no. 2, pp. 89–144, 1998.
- [18] K. J. Edgar, "Cellulose esters in drug delivery," *Cellulose*, vol. 14, no. 1, pp. 49–64, 2007.
- [19] J. Fu, Z. Pang, J. Yang, F. Huang, Y. Cai, and Q. Wei, "Fabrication of polyaniline/carboxymethyl cellulose/cellulose nanofibrous mats and their biosensing application," *Appl. Surf. Sci.*, vol. 349, pp. 35–42, 2015.
- [20] W.-S. Huang, B. D. Humphrey, and A. G. MacDiarmid, "Polyaniline, a novel conducting polymer. Morphology and chemistry of its oxidation and reduction in aqueous electrolytes," *J. Chem. Soc. Faraday Trans. 1 Phys. Chem. Condens. Phases*, vol. 82, no. 8, p. 2385, 1986.
- [21] Z. A. Boeva and V. G. Sergeev, "Polyaniline: Synthesis, properties, and application," *Polym. Sci. Ser. C*, vol. 56, no. 1, pp. 144–153, 2014.
- [22] on Efimov and T. Vernitskaya, "Polypyrrole: a conducting polymer; its synthesis, properties and applications," *Russ. Chem. Rev.*, vol. 66, no. 5, pp. 443–457, 1997.
- [23] S. V. Selvaganesh, J. Mathiyarasu, K. L. N. Phani, and V. Yegnaraman, "Chemical synthesis of PEDOT-Au nanocomposite," *Nanoscale Res. Lett.*, vol. 2, no. 11, pp. 546–549, 2007.

- [24] K. Sun *et al.*, "Review on application of PEDOTs and PEDOT:PSS in energy conversion and storage devices," *J. Mater. Sci. Mater. Electron.*, vol. 26, no. 7, pp. 4438–4462, 2015.
- [25] E. N. Prasetyo, S. Semlitsch, G. S. Nyanhongo, Y. Lemmouchi, and G. M. Guebitz, "Laccase functionalized cellulose acetate for the removal of toxic combustion products," *React. Funct. Polym.*, vol. 97, no. December, pp. 12–18, 2015.
- [26] Z. M. Huang, Y. Z. Zhang, M. Kotaki, and S. Ramakrishna, "A review on polymer nanofibers by electrospinning and their applications in nanocomposites," *Compos. Sci. Technol.*, vol. 63, no. 15, pp. 2223–2253, 2003.
- [27] R. D. Velasco Barraza, A. S. Álvarez Suarez, L. J. Villarreal Gómez, J. A. Paz González, A. L. Iglesias, and R. Vera Graziano, "Designing a low cost electrospinning device for practical learning in a Bioengineering Biomaterials course," *Rev. Mex. Ing. Biomed.*, vol. 37, no. 1, pp. 7–16, 2016.
- [28] A. C. B. Baptista, "Development of bio-batteries based on electrospun membranes," 2014.
- [29] E. Barsoukov and J. R. Macdonald, *Impedance Spectroscopy*. 2005.
- [30] B.-Y. Chang and S.-M. Park, "Electrochemical Impedance Spectroscopy," *Annu. Rev. Anal. Chem.*, vol. 3, no. 1, pp. 207–229, 2010.
- [31] A. Mena-Bravo and M. D. Luque de Castro, "Sweat: A sample with limited present applications and promising future in metabolomics," *J. Pharm. Biomed. Anal.*, vol. 90, pp. 139–147, 2014.
- [32] E. Cho, M. Mohammadifar, and S. Choi, "A self-powered sensor patch for glucose monitoring in sweat," *Proc. IEEE Int. Conf. Micro Electro Mech. Syst.*, pp. 366–369, 2017.
- [33] M. Zhou and J. Wang, "Biofuel Cells for Self-Powered Electrochemical Biosensing and Logic Biosensing: A Review," *Electroanalysis*, vol. 24, no. 2, pp. 197–209, 2012.
- [34] A. R. Stoyanova and V. T. Tsakova, "Electrooxidation of glucose on copper-modified polyaniline layers in alkaline solution," *Bulg. Chem. Commun.*, vol. 40, no. 3, pp. 286–290, 2008.
- [35] T. S. et al Masato Tominaga, "Electro-catalytic oxidation of glucose at carbon electrodes modified with gold and gold-platinum alloy nanoparticles in an alkaline solution," *Chem. Lett.*, vol. 34, no. 2, pp. 202–203, 2005.
- [36] E. I. Gill, A. Arshak, K. Arshak, and O. Korostynska, "Novel conducting polymer composite pH sensors for medical applications," *IFMBE Proc.*, vol. 20 IFMBE, pp. 225–228, 2008.
- [37] U. Schmidt, M. Guenther, and G. Gerlach, "Biochemical piezoresistive

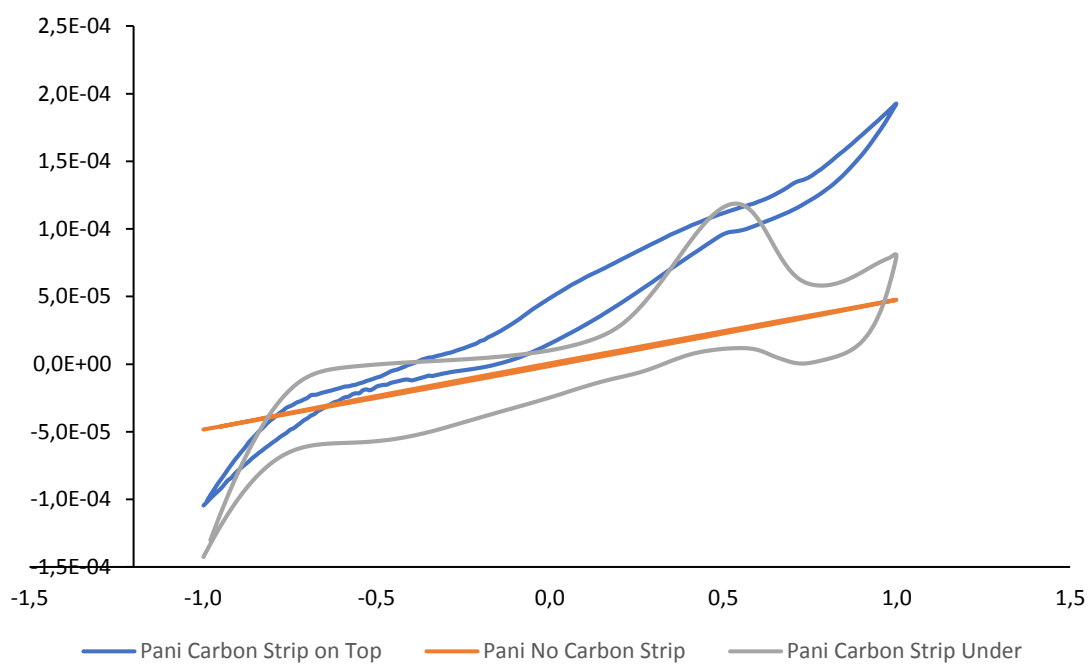
- sensors based on pH- and glucose-sensitive hydrogels for medical applications," *Curr. Dir. Biomed. Eng.*, vol. 2, no. 1, pp. 117–121, 2016.
- [38] K. Kulthong, S. Srisung, K. Boonpavanitchakul, W. Kangwansupamonkon, and R. Maniratanachote, "Determination of silver nanoparticle release from antibacterial fabrics into artificial sweat," *Part. Fibre Toxicol.*, vol. 7, no. 1, p. 8, 2010.
- [39] C. Callewaert, B. Buyschaert, E. Vossen, V. Fievez, T. Van de Wiele, and N. Boon, "Artificial sweat composition to grow and sustain a mixed human axillary microbiome," *J. Microbiol. Methods*, vol. 103, pp. 6–8, 2014.
- [40] P. T. Kissinger and W. R. Heineman, "Cyclic voltammetry," *J. Chem. Educ.*, vol. 60, no. 9, pp. 9242–5, 1983.
- [41] H. S. Barud *et al.*, "Thermal behavior of cellulose acetate produced from homogeneous acetylation of bacterial cellulose," *Thermochim. Acta*, vol. 471, no. 1–2, pp. 61–69, 2008.
- [42] H. Liu and Y. Lo Hsieh, "Ultrafine fibrous cellulose membranes from electrospinning of cellulose acetate," *J. Polym. Sci. Part B Polym. Phys.*, vol. 40, no. 18, pp. 2119–2129, 2002.
- [43] M. da C. C. Lucena, A. E. V De Alencar, S. E. Mazzeto, and S. de A. Soares, "The effect of additives on the thermal degradation of cellulose acetate," *Polym. Degrad. Stab.*, vol. 80, no. 1, pp. 149–155, 2003.
- [44] Z. Osman and A. K. Arof, "FTIR studies of chitosan acetate based polymer electrolytes," *Electrochim. Acta*, vol. 48, no. 8, pp. 993–999, 2003.
- [45] M. Trchová, I. Šeděnková, E. Tobolková, and J. Stejskal, "FTIR spectroscopic and conductivity study of the thermal degradation of polyaniline films," *Polym. Degrad. Stab.*, vol. 86, no. 1, pp. 179–185, 2004.
- [46] X. Du, H.-Y. Liu, G. Cai, Y.-W. Mai, and A. Baji, "Use of facile mechanochemical method to functionalize carbon nanofibers with nanostructured polyaniline and their electrochemical capacitance.," *Nanoscale Res. Lett.*, vol. 7, no. 1, p. 111, 2012.
- [47] S. K. Dhawan, D. Kumar, M. K. Ram, S. Chandra, and D. C. Trivedi, "Application of conducting polyaniline as sensor material for ammonia," *Sensors Actuators B Chem.*, vol. 40, no. 2–3, pp. 99–103, 1997.
- [48] H. Yamato, M. Ohwa, and W. Wernet, "Stability of polypyrrole and poly(3,4-ethylenedioxythiophene) for biosensor application," *J. Electroanal. Chem.*, vol. 397, no. 1–2, pp. 163–170, 1995.
- [49] D. A. Harrington and P. Van Den Driessche, "Mechanism and equivalent circuits in electrochemical impedance spectroscopy," *Electrochim. Acta*, vol. 56, no. 23, pp. 8005–8013, 2011.
- [50] M. Baghayeri and M. Namadchian, "Fabrication of a nanostructured

- luteolin biosensor for simultaneous determination of levodopa in the presence of acetaminophen and tyramine: Application to the analysis of some real samples," *Electrochim. Acta*, vol. 108, no. Supplement C, pp. 22–31, 2013.
- [51] Y. Ding, Y. Wang, L. Su, H. Zhang, and Y. Lei, "Preparation and characterization of NiO–Ag nanofibers, NiO nanofibers, and porous Ag: towards the development of a highly sensitive and selective non-enzymatic glucose sensor," *J. Mater. Chem.*, vol. 20, no. 44, p. 9918, 2010.
- [52] K. R. Prasad and N. Munichandraiah, "Electrocatalytic efficiency of polyaniline by cyclic voltammetry and electrochemical impedance spectroscopy studies," *Synth. Met.*, vol. 126, no. 1, pp. 61–68, 2002.
- [53] J. Moyer, D. Wilson, I. Finkelshtein, B. Wong, and R. Potts, "Correlation Between Sweat Glucose and Blood Glucose in Subjects with Diabetes," *Diabetes Technol. Ther.*, vol. 14, no. 5, pp. 398–402, 2012.
- [54] K. Sakaguchi *et al.*, "Evaluation of a minimally invasive system for measuring glucose area under the curve during oral glucose tolerance tests: Usefulness of sweat monitoring for precise measurement," *J. Diabetes Sci. Technol.*, vol. 7, no. 3, pp. 678–688, 2013.
- [55] J. Chen, H. Zheng, J. Kang, F. Yang, Y. Cao, and M. Xiang, "An alkaline direct oxidation glucose fuel cell using three-dimensional structural Au/Ni-foam as catalytic electrodes," *RSC Adv.*, vol. 7, no. 5, pp. 3035–3042, 2017.
- [56] Z. Fan *et al.*, "A flexible and disposable hybrid electrode based on Cu nanowires modified graphene transparent electrode for non-enzymatic glucose sensor," *Electrochim. Acta*, vol. 109, no. 0, pp. 602–608, 2013.
- [57] M. Baghayeri, A. Amiri, and S. Farhadi, "Development of non-enzymatic glucose sensor based on efficient loading Ag nanoparticles on functionalized carbon nanotubes," *Sensors Actuators, B Chem.*, vol. 225, pp. 354–362, 2016.

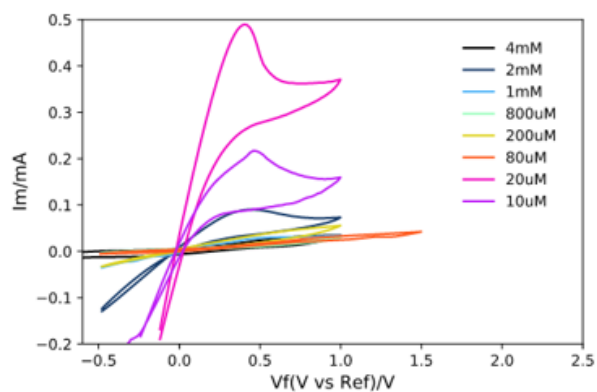
6

Appendices

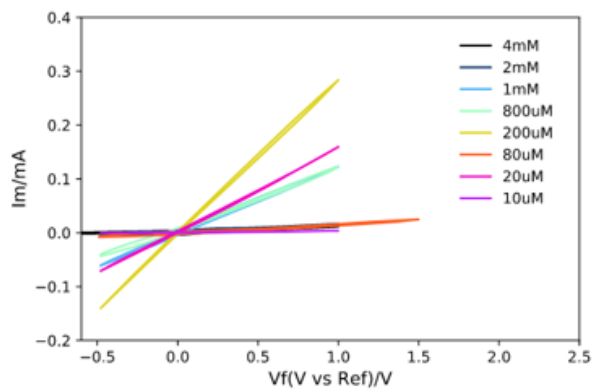
Appendix A.1 – Cyclic Voltammetry Experimental Setup Results without a Carbon strip inside the Teflon-made cell, with a carbon strip on top of the membrane and beneath it



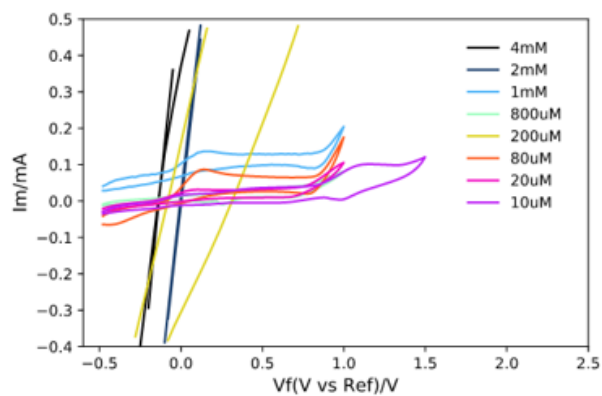
Appendix A.2 -Cyclic Voltammograms for PANI/CA, PPy/CA and PE-DOT/CA using differently concentrated solutions of glucose electrolyte



(i)

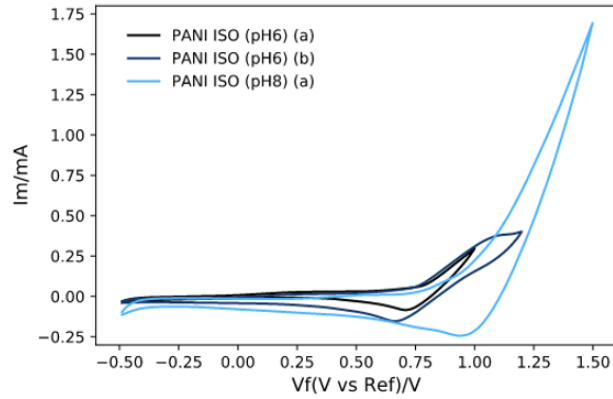


(ii)

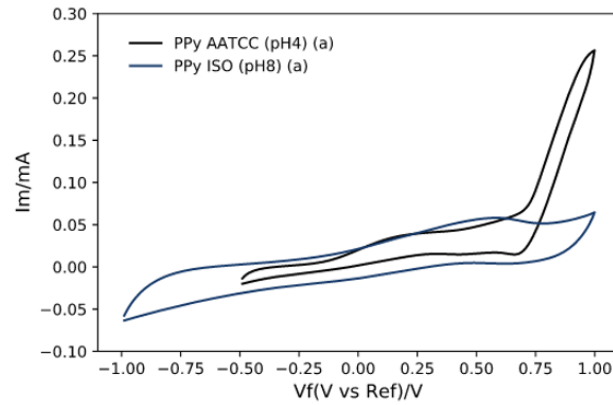


(iii)

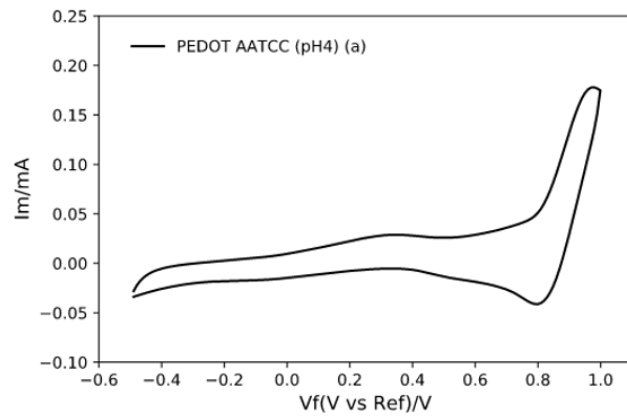
Appendix A.3 - Artificial Sweat Cyclic Voltammetry of PANI/CA, PPy/CA and PEDOT/CA with different ranges of applied potential



(i)



(ii)



(iii)

Appendix A.4 – Chronoamperometry for PANI/CA with Artificial Sweat Solutions testing different methodologies

